

Four-nucleon scattering with a correlated Gaussian basis method

S. Aoyama¹, K. Arai², Y. Suzuki^{3,4}, P. Descouvemont⁵, D. Baye^{6,5}

¹ Center for Academic Information Service, Niigata University, Niigata 950-2181, Japan

² Division of General Education, Nagaoka National College of Technology, 888 Nishikataikai, Nagaoka, Niigata, 940-8532, Japan

³ Department of Physics, Niigata University, Niigata 950-2181, Japan

⁴ RIKEN Nishina Center, RIKEN, Wako 351-0198, Japan

⁵ Physique Nucléaire Théorique et Physique Mathématique, C.P. 229, Université Libre de Bruxelles (ULB), B 1050 Brussels, Belgium

⁶ Physique Quantique, C.P. 165/82, Université Libre de Bruxelles (ULB), B 1050 Brussels, Belgium

Abstract. Elastic-scattering phase shifts for four-nucleon systems are studied in an *ab-initio* type cluster model in order to clarify the role of the tensor force and to investigate cluster distortions in low energy $d+d$ and $t+p$ scattering. In the present method, the description of the cluster wave function is extended from a simple ($0s$) harmonic-oscillator shell model to a few-body model with a realistic interaction, in which the wave function of the subsystems are determined with the Stochastic Variational Method. In order to calculate the matrix elements of the four-body system, we have developed a Triple Global Vector Representation method for the correlated Gaussian basis functions. To compare effects of the cluster distortion with realistic and effective interactions, we employ the AV8' potential as a realistic interaction and the Minnesota potential as an effective interaction. Especially for 1S_0 , the calculated phase shifts show that the $t+p$ and $h+n$ channels are strongly coupled to the $d+d$ channel for the case of the realistic interaction. On the contrary, the coupling of these channels plays a relatively minor role for the case of the effective interaction. This difference between both potentials originates from the tensor term in the realistic interaction. Furthermore, the tensor interaction makes the energy splitting of the negative parity states of ^4He consistent with experiments. No such splitting is however reproduced with the effective interaction.

1 Introduction

The microscopic cluster model is one of the successful models to study the structure and reactions of light nuclei [1]. In the conventional cluster model, one

assumes that the nucleus is composed of several simple clusters with $A \leq 4$ which are described by (0s) harmonic-oscillator shell model functions, and use an effective N - N interaction which is appropriate for such a model space. However, it is well known that the ground states of the typical clusters d , t , h and ${}^4\text{He}$ have non-negligible admixtures of D -wave component due to the tensor interaction. Since the conventional cluster model does not directly treat the D -wave component, the strong attraction of the nucleon-nucleon interaction due to the tensor term is assumed to be renormalized into the central term of the effective interaction.

Recently, *ab-initio* structure calculations [2] have been successfully developed: Stochastic Variational Method (SVM) [3, 4, 5, 6], Global Vector Representation method (GVR) [7, 8], Green's function Monte Carlo method [9], no core shell model [10], correlated hyperspherical harmonics method [11], unitary correlation operator method [12], and so on. Although the application of *ab-initio* reaction calculations with a realistic interaction are restricted so much in comparison with structure calculations, it has been intensively applied to the four-nucleon systems $t+n$ and $h+p$ [13, 14, 15, 16, 17, 18, 19]. Especially $d+d$ scattering states, which couple to $t+p$ and $h+n$ channels, have attracted much attention, because the $d+d$ radiative capture is one of the mechanisms making ${}^4\text{He}$ through electromagnetic transitions [20, 21] and also have posed intriguing puzzles for analyzing powers [22, 23, 24, 25, 26], which are motivated by the famous A_y problem in the three-nucleon system.

Furthermore, the $d+d$ elastic-scattering phase shifts are interesting because the astrophysical S-factor of the $d(d,\gamma){}^4\text{He}$ reaction is not explained by any calculation using an effective interaction that contains no tensor term, and is expected to be contributed by the D -wave components of the clusters through $E2$ transitions [27, 28].

Also, thanks to recent developments of the microscopic cluster model, the simple model using the (0s) harmonic-oscillator wave function with an effective interaction is not mandatory any more, at least, in light nuclei. We can use a kind of *ab-initio* cluster model which employs more realistic cluster wave functions with realistic interactions. Therefore, it is interesting to see the difference between the *ab-initio* reaction calculations with a tensor term and the conventional cluster model calculations without a tensor term in few-body systems.

The microscopic R -matrix method (MRM) with a cluster model (GCM or RGM) has been applied to studies of many nuclei [29, 30, 31, 32]. It is now used in *ab initio* descriptions of collisions [16]. We have also applied the MRM to the $h+p$ scattering problem with more realistic cluster wave functions by using a realistic interaction [13]. The Gaussian basis functions for the expansion of the cluster wave functions are chosen by a technique of the SVM [5]. In the MRM, as will be shown later, the relative wave function between clusters (a and b) is connected to the boundary condition at a channel radius. The problem is how to calculate the matrix elements. In this paper, we develop a method called the Triple Global Vector Representation method (TGVR), by which we calculate the matrix elements in a unified way. Although we restricted ourselves to four nucleon systems in the present paper, the formulation of the TGVR itself can

be applied to more than four-body systems as in the previous studies of the Global Vector Representation methods (GVR) [8]. Furthermore, for scattering problems, the TGVR can deal with more complicated systems than the double (or single) global vector which was given in the previous papers [7, 8], because we need three representative orbital angular momenta, the total internal orbital momenta of both clusters and the orbital momentum of their relative motion, in order to reasonably describe the scattering states. In other words, the first global vector represents the angular momentum of cluster a , the second global vector represents the angular momentum of cluster b , and the third global vector represents the relative angular momentum between the clusters.

In this paper, we will investigate the effect of the distortion of clusters on the $d+d$ elastic-scattering by comparing the phase shifts calculated with a realistic and an effective interaction. In section 2, we explain the MRM in brief. In section 3, the correlated Gaussian (CG) method with the TGVR, which has newly been developed for the present analysis, will be presented. In section 4, we will explain how to calculate the matrix elements with TGVR basis functions. The typical matrix elements are also given in the appendix. In section 5, we will present and discuss the calculated scattering phase shifts in detail. Finally, summary and conclusions are given in section 6.

2 Microscopic R -matrix method

In the present study we calculate $d+d$ and $t+p$ (and $h+n$) elastic scattering phase shifts with the microscopic R -matrix method. Though the method is well documented in e.g. Refs. [29, 30, 32], we briefly explain it below in order to present definitions and equations needed in the subsequent sections. Since our interest is on low-energy scattering, we consider only two-body channels. A channel α is specified by the two nuclei (clusters) a, b , their angular momenta, I_a, I_b , the channel spin I that is a resultant of the coupling of I_a and I_b , and the orbital angular momentum ℓ for the relative motion of a and b . The wave function of channel α with the total angular momentum J , its projection M , and the parity π takes the form

$$\Psi_\alpha^{JM\pi} = \mathcal{A} \left[\left[\Phi_{I_a}^a \Phi_{I_b}^b \right]_I \chi_\alpha(\rho_\alpha) \right]_{JM}, \quad (2.1)$$

where $\Phi_{I_a}^a$ and $\Phi_{I_b}^b$ are respectively antisymmetrized intrinsic wave functions of a and b , and \mathcal{A} is an operator that antisymmetrizes between the clusters. The square bracket $[I_a I_b]_I$ denotes the angular momentum coupling. The coordinate ρ_α in the relative motion function χ_α^J is the relative distance vector of the clusters. The channel spin I and the relative angular momentum ℓ in α are coupled to give the total angular momentum J . The relative-motion functions χ_α also depend on J and π . For simplicity, this dependence is not displayed explicitly in the notation for χ_α as well as for some other quantities below.

The configuration space is divided into two regions, internal and external, by the channel radius a . In the internal region ($\rho_\alpha \leq a$), the total wave function

may be expressed in terms of a combination of various $\Psi_\alpha^{JM\pi}$ s

$$\begin{aligned}\Psi_{\text{int}}^{JM\pi} &= \sum_{\alpha} \Psi_{\alpha}^{JM\pi} \\ &= \sum_{\alpha} \sum_n f_{\alpha n} \mathcal{A} u_{\alpha n}(\rho_{\alpha}) \phi_{\alpha}^{JM\pi},\end{aligned}\quad (2.2)$$

with

$$\begin{aligned}\phi_{\alpha}^{JM\pi} &= \frac{1}{\sqrt{(1 + \delta_{I_a I_b} \delta_{ab})(1 + \delta_{ab})}} \left\{ \left[\left[\Phi_{I_a}^a \Phi_{I_b}^b \right]_I Y_{\ell}(\widehat{\boldsymbol{\rho}}_{\alpha}) \right]_{JM} \right. \\ &\quad \left. + (-1)^{A_a + I_a + I_b - I + \ell} \left[\left[\Phi_{I_b}^b \Phi_{I_a}^a \right]_I Y_{\ell}(\widehat{\boldsymbol{\rho}}_{\alpha}) \right]_{JM} \delta_{ab} \right\},\end{aligned}\quad (2.3)$$

where A_a is the number of nucleons in cluster a , δ_{ab} is unity if a and b are identical clusters and zero otherwise, and $\delta_{I_a I_b}$ is unity if the clusters are in identical states and zero otherwise. In the second line of Eq. (2.2), the relative motion functions of Eq. (2.1) are expanded in terms of some basis functions as

$$\chi_{\alpha m}(\boldsymbol{\rho}_{\alpha}) = \sum_n f_{\alpha n} u_{\alpha n}(\rho_{\alpha}) Y_{\ell m}(\widehat{\boldsymbol{\rho}}_{\alpha}).\quad (2.4)$$

In what follows we take

$$u_{\alpha n}(\rho_{\alpha}) = \rho_{\alpha}^{\ell} \exp\left(-\frac{1}{2} \lambda_n \rho_{\alpha}^2\right)\quad (2.5)$$

with a suitable set of λ_n s.

In the external region ($\rho_{\alpha} \geq a$), the total wave function takes the form

$$\Psi_{\text{ext}}^{JM\pi} = \sum_{\alpha} g_{\alpha}(\rho_{\alpha}) \phi_{\alpha}^{JM\pi}.\quad (2.6)$$

Note that the antisymmetrization between the clusters is dropped in the external region under the condition that the channel radius a is large enough. The function $g_{\alpha}(\rho_{\alpha})$ of Eq. (2.6) is a solution of the equation

$$\left[-\frac{\hbar^2}{2\mu_{\alpha}} \left(\frac{d^2}{d\rho_{\alpha}^2} + \frac{2}{\rho_{\alpha}} \frac{d}{d\rho_{\alpha}} - \frac{\ell(\ell+1)}{\rho_{\alpha}^2} \right) + \frac{Z_a Z_b e^2}{\rho_{\alpha}} \right] g_{\alpha}(\rho_{\alpha}) = E_{\alpha} g_{\alpha}(\rho_{\alpha}),\quad (2.7)$$

where μ_{α} is the reduced mass for the relative motion in channel α , $Z_a e$ and $Z_b e$ are the charges of a and b , and $E_{\alpha} = E - E_a - E_b$ is the energy for the relative motion, where E is the total energy, and E_a and E_b are the internal energies for the clusters a and b , respectively. For the scattering initiated through the channel α_0 , the asymptotic form of g_{α} for the open channel α ($E_{\alpha} \geq 0$) is

$$g_{\alpha}(\rho_{\alpha}) = v_{\alpha}^{-1/2} \rho_{\alpha}^{-1} [I_{\alpha}(k_{\alpha} \rho_{\alpha}) \delta_{\alpha \alpha_0} - S_{\alpha \alpha_0}^{J\pi} O_{\alpha}(k_{\alpha} \rho_{\alpha})],\quad (2.8)$$

where $k_{\alpha} = \sqrt{2\mu_{\alpha}|E_{\alpha}|}/\hbar$, $v_{\alpha} = \hbar k_{\alpha}/\mu_{\alpha}$ and $S_{\alpha \alpha_0}^{J\pi}$ is an element of the S -matrix (or collision matrix) to be determined. Here $I_{\alpha}(k_{\alpha} \rho_{\alpha})$ and $O_{\alpha}(k_{\alpha} \rho_{\alpha})$ are the incoming and outgoing waves defined by

$$I_{\alpha}(k_{\alpha} \rho_{\alpha}) = O_{\alpha}(k_{\alpha} \rho_{\alpha})^* = G_{\ell}(\eta_{\alpha}, k_{\alpha} \rho_{\alpha}) - iF_{\ell}(\eta_{\alpha}, k_{\alpha} \rho_{\alpha}),\quad (2.9)$$

with the regular and irregular Coulomb functions F_ℓ and G_ℓ . The Sommerfeld parameter η_α is $\mu_\alpha Z_a Z_b e^2 / \hbar^2 k_\alpha$. For a closed channel α ($E_\alpha < 0$), the asymptotic form of g_α is given by the Whittaker function

$$g_\alpha(\rho_\alpha) \propto \rho_\alpha^{-1} W_{-\eta_\alpha, \ell+1/2}(2k_\alpha \rho_\alpha). \quad (2.10)$$

The matrix elements $S_{\alpha\alpha_0}^{J\pi}$ are determined by solving a Schrödinger equation with a microscopic Hamiltonian H involving the $A_a + A_b$ nucleons,

$$(H + \mathcal{L} - E)\Psi_{\text{int}}^{JM\pi} = \mathcal{L}\Psi_{\text{ext}}^{JM\pi}, \quad (2.11)$$

with the Bloch operator \mathcal{L}

$$\mathcal{L} = \sum_\alpha \frac{\hbar^2}{2\mu_\alpha a} |\phi_\alpha^{JM\pi}\rangle \delta(\rho_\alpha - a) \left(\frac{\partial}{\partial \rho_\alpha} - \frac{b_\alpha}{\rho_\alpha} \right) \rho_\alpha \langle \phi_\alpha^{JM\pi}|, \quad (2.12)$$

where the channel radius a is chosen to be the same for all channels, and the b_α are arbitrary constants. Here, we choose $b_\alpha = 0$ for the open channels and $b_\alpha = 2k_\alpha a W'_{-\eta_\alpha, \ell+1/2}(2k_\alpha a) / W_{-\eta_\alpha, \ell+1/2}(2k_\alpha a)$ for the closed channels. The results do not depend on the choices for b_α but these values simplify the calculations. Notice that the projector on $|\phi_\alpha^{JM\pi}\rangle$ in Eq. (2.12) is not essential in a microscopic calculation and can be dropped since the various channels are orthogonal at the channel radius.

The Bloch operator ensures that the logarithmic derivative of the wave function is continuous at the channel radius. In addition, $\Psi_{\text{int}}^{JM\pi}$ must be equal to $\Psi_{\text{ext}}^{JM\pi}$ at $\rho_\alpha = a$. Projecting the Schrödinger equation on a basis state, one obtains

$$\sum_{\alpha n} C_{\alpha' n', \alpha n} f_{\alpha n} = \langle \Phi_{\alpha' n'}^{JM\pi} | \mathcal{L} | \Psi_{\text{ext}}^{JM\pi} \rangle \quad (2.13)$$

with

$$C_{\alpha' n', \alpha n} = \langle \Phi_{\alpha' n'}^{JM\pi} | H + \mathcal{L} - E | \mathcal{A} \Phi_{\alpha n}^{JM\pi} \rangle_{\text{int}}, \quad (2.14)$$

and

$$\Phi_{\alpha n}^{JM\pi} = u_{\alpha n}(\rho_\alpha) \phi_\alpha^{JM\pi}. \quad (2.15)$$

Here $\langle |\mathcal{O}| \rangle_{\text{int}}$ indicates that the integration with respect to ρ_α is to be carried out in the internal region. Actually $\langle |\mathcal{O}| \rangle_{\text{int}}$ is obtained by calculating the matrix element $\langle |\mathcal{O}| \rangle$ in the entire space and subtracting the corresponding external matrix element $\langle |\mathcal{O}| \rangle_{\text{ext}}$ that is easily obtained because no intercluster antisymmetrization is needed. The R -matrix and Z -matrix are defined by

$$\mathcal{R}_{\alpha' \alpha} \equiv \frac{\hbar^2 a}{2} \left(\frac{k_{\alpha'}}{\mu_{\alpha'} \mu_\alpha k_\alpha} \right)^{\frac{1}{2}} \sum_{n' n} u_{\alpha' n'}(a) (C^{-1})_{\alpha' n', \alpha n} u_{\alpha n}(a), \quad (2.16)$$

$$\mathcal{Z}_{\alpha' \alpha} \equiv I_\alpha(k_\alpha a) \delta_{\alpha' \alpha} - \mathcal{R}_{\alpha' \alpha} k_\alpha a I'_\alpha(k_\alpha a). \quad (2.17)$$

The S -matrix is finally obtained as

$$S^{J\pi} = (\mathcal{Z}^*)^{-1} \mathcal{Z}. \quad (2.18)$$

Table 1. Channel spins ($^{2I+1}\ell_J$) of physical $d+d$, $t+p$, and $h+n$ channels for $J \leq 2$ and $\ell \leq 2$.

channel	J^π					
	0^+	1^+	2^+	0^-	1^-	2^-
$d(1^+)+d(1^+)$	1S_0 5D_0	5D_1	5S_2 1D_2 5D_2	3P_0	3P_1	3P_2
$t(\frac{1}{2}^+)+p(\frac{1}{2}^+), h(\frac{1}{2}^+)+n(\frac{1}{2}^+)$	1S_0	3S_1 3D_1	1D_2 3D_2	3P_0	1P_1 3P_1	3P_2

In this paper we focus on the elastic phase shifts $\delta_\alpha^{J\pi}$ that are defined by the diagonal elements of the S -matrix,

$$S_{\alpha\alpha}^{J\pi} = \eta_\alpha^{J\pi} e^{2i\delta_\alpha^{J\pi}}. \quad (2.19)$$

We study four-nucleon scattering involving the $d+d$, $t+p$ and $h+n$ channels in the energy region around and below the $d+d$ threshold. In Table 1 we list all possible labels $^{2I+1}\ell_J$ of physical channels for $J^\pi = 0^\pm, 1^\pm, \text{ and } 2^\pm$, assuming $\ell \leq 2$. Here ‘‘physical’’ means that the channels involve the cluster bound states that appear in the external region as well. Non-physical channels involving excited pseudo states will also be included in most calculations. Note that the $d+d$ channel must satisfy the condition of $I + \ell$ even (see Eq. (2.3)). The channel spin $I = 0$ or 2 can couple with only even ℓ , but $I = 1$ with only odd ℓ . It is noted that the relative motion for the $d+d$ scattering can have $\ell = 0$ only when J^π is equal to 0^+ and 2^+ .

Because one of our purposes in this investigation is to understand the role of the tensor force played in the four-nucleon dynamics, we want to compare the phase shifts obtained with two Hamiltonians that differ in the type of NN interactions. One is a realistic interaction called the AV8' potential [33] that includes central, tensor and spin-orbit components. We also add an effective three-nucleon force (TNF) in order to reproduce reasonably the binding energies of t , h and ^4He [34], which makes reasonable thresholds. In the present calculation, the TNF is included in all calculations for AV8'. Another is an effective central interaction called the Minnesota (MN) potential [35], which reproduce reasonably the binding energies of t , h and ^4He , though it has central terms alone (with an exchange parameter $u = 1$). The Coulomb potential is included for both potentials.

The intrinsic wave function $\Phi_{I_k}^k$ of cluster k ($k = a, b$) is described with a combination of N_k basis functions with different L_k and S_k values

$$\Phi_{I_k M_{I_k}}^k = \sum_{N_k} \mathcal{A} \left[\psi_{L_k}^{(\text{space})} \psi_{S_k}^{(\text{spin})} \right]_{I_k M_{I_k}} \psi_{T_k M_{T_k}}^{(\text{isospin})}, \quad (2.20)$$

where $\psi_{L_k}^{(\text{space})}$, $\psi_{S_k}^{(\text{spin})}$ and $\psi_{T_k M_{T_k}}^{(\text{isospin})}$ denote the space, spin and isospin parts of the cluster wave function. In the case of the AV8' potential, the t (or h) wave function is approximated with thirty Gaussian basis functions that include $L_k \leq 2$,

Table 2. Energies E , rms radii R^{rms} and D -state probabilities P_D of the clusters that appear in four-nucleon scattering and ${}^4\text{He}$ with the AV8' (with TNF) and MN potentials. N_k is the number of basis functions used to approximate the wave function of cluster k . The values in the last three columns for three- and four-body systems are taken from Ref. [34] for AV8' and Ref. [7] for MN.

potential	cluster	N_k	present			literature		
			E (MeV)	R^{rms} (fm)	P_D (%)	E (MeV)	R^{rms} (fm)	P_D (%)
AV8' (with TNF)	$d(1^+)$	8	-2.18	1.79	5.9	-2.24	1.96	5.8
	$t(\frac{1}{2}^+)$	30	-8.22	1.69	8.4	-8.41	-	-
	$h(\frac{1}{2}^+)$	30	-7.55	1.71	8.3	-7.74	-	-
	${}^4\text{He}(0^+)$	(2370)	-27.99	1.46	13.8	-28.44	-	14.1
MN	$d(1^+)$	4	-2.10	1.63	0	-2.20	1.95	0
	$t(\frac{1}{2}^+)$	15	-8.38	1.70	0	-8.38	1.71	0
	$h(\frac{1}{2}^+)$	15	-7.70	1.72	0	-7.71	1.74	0
	${}^4\text{He}(0^+)$	(1140)	-29.94	1.41	0	-29.94	1.41	0

and $S_k = \frac{1}{2}$ and $\frac{3}{2}$. The deuteron wave function is also approximated with Gaussian basis functions, four terms both in the S - and D -waves, respectively. The falloff parameters of the Gaussian functions are selected using the SVM [5] and the expansion coefficients are determined by diagonalizing the intrinsic cluster Hamiltonian. A similar procedure is applied to the case of the MN potential.

The calculated energies E , root-mean-square (rms) radii R^{rms} and D state probabilities P_D are given in the fourth to sixth columns in Table 2. We use the truncated basis in order to obtain the phase shifts in reasonable computer times, they slightly deviate from more elaborate calculations, which are given in the last three columns. Fortunately, except for the small shift of the threshold energy, the phase shifts are not very sensitive to the details of the cluster wave functions because they are determined by the change of the relative motion function of the clusters. The N_k values in parenthesis for ${}^4\text{He}$ are the number of $J^\pi = 0^+$ basis functions in the major multi-channel calculation. The energy of ${}^4\text{He}$ calculated in Table 2 with the multi-channel calculation is thus not optimized but found to be very close to that of the more extensive calculation. It is noted that the calculated R^{rms} value for the deuteron is smaller than in other calculations. This is due to the restricted choice of the length parameters of the basis functions, which permits us to use a relatively small channel radius of $a \sim 15$ fm. We have checked that the phase shifts for a $d+d$ single channel calculation do not change even when more extended deuteron wave functions are employed.

3 Correlated Gaussian function with triple global vectors

As explained in the previous section, the calculation of the S -matrix reduces to that of the Hamiltonian and overlap matrix elements with the functions defined by (2.1) and (2.20), and it is conveniently performed by transforming that wave function into an LS -coupled form,

$$\mathcal{A} \left[\left[\left[\psi_{L_a}^{(\text{space})} \psi_{L_b}^{(\text{space})} \right]_{L_{ab}} \chi_\alpha(\boldsymbol{\rho}_\alpha) \right]_L \left[\psi_{S_a}^{(\text{spin})} \psi_{S_b}^{(\text{spin})} \right]_S \right]_{JM}. \quad (3.1)$$

The transformation can be done as

$$\begin{aligned} & \mathcal{A} \left[\left[\left[\psi_{L_a}^{(\text{space})} \psi_{S_a}^{(\text{spin})} \right]_{I_a} \left[\psi_{L_b}^{(\text{space})} \psi_{S_b}^{(\text{spin})} \right]_{I_b} \right]_I \chi_\alpha(\boldsymbol{\rho}_\alpha) \right]_{JM} \psi_{T_a M_{T_a}}^{(\text{isospin})} \psi_{T_b M_{T_b}}^{(\text{isospin})} \\ &= \sum_{L_{ab} L S} \begin{bmatrix} L_a & S_a & I_a \\ L_b & S_b & I_b \\ L_{ab} & S & I \end{bmatrix} (-1)^{L_{ab}+J-I-L} U(SL_{ab} J \ell; I L) \\ & \times \mathcal{A} \left[\psi_{L_a L_b (L_{ab}) \ell L}^{(\text{space})} \left[\psi_{S_a}^{(\text{spin})} \psi_{S_b}^{(\text{spin})} \right]_S \right]_{JM} \psi_{T_a M_{T_a}}^{(\text{isospin})} \psi_{T_b M_{T_b}}^{(\text{isospin})} \end{aligned} \quad (3.2)$$

with

$$\psi_{L_a L_b (L_{ab}) \ell L}^{(\text{space})} = \left[\left[\psi_{L_a}^{(\text{space})} \psi_{L_b}^{(\text{space})} \right]_{L_{ab}} \chi_\alpha(\boldsymbol{\rho}_\alpha) \right]_L, \quad (3.3)$$

where U and $[\]$ are Racah and $9j$ coefficients in unitary form [5].

The evaluation of the matrix element can be done in the spatial, spin, and isospin parts separately. The spin and isospin parts are obtained straightforwardly. In the following we concentrate on the spatial matrix element. The spatial part (3.3) of the total wave function is given as a product of the cluster intrinsic parts and their relative motion part. The coordinates used to describe the $2N+2N$ channel are depicted in Fig. 1(a) with $\boldsymbol{\rho}_\alpha = \boldsymbol{x}_3$, whereas the coordinates suitable for the $t+p$ and $h+n$ channels are shown in Fig. 1(b) with $\boldsymbol{\rho}_\alpha = \boldsymbol{x}'_3$. These coordinate sets are often called H-type and K-type. Therefore the calculation of the spatial matrix element requires a coordinate transformation involving the angular momenta L_a, L_b, ℓ and L_{ab} . Moreover the permutation operator in \mathcal{A} causes a complicated coordinate transformation. All these complexities are treated elegantly by introducing a correlated Gaussian [36, 6, 5], provided each part of $\psi_{L_a L_b (L_{ab}) \ell L}^{(\text{space})}$ is given in terms of (a combination of) Gaussian functions as in the present case. In what follows we will demonstrate how it is performed. Because the formulation with the correlated Gaussian is not restricted to four nucleons but can be applied to a system including more particles, the number of nucleons is assumed to be N in this and next sections as well as in Appendices B and C unless otherwise mentioned.

The relative and center of mass coordinates of the N nucleons, \boldsymbol{x}_i ($i = 1, \dots, N$), and the single-particle coordinates, \boldsymbol{r}_i ($i = 1, \dots, N$), are mutually related by a linear transformation matrix U and its inverse U^{-1} as follows:

$$\boldsymbol{x}_i = \sum_{j=1}^N U_{ij} \boldsymbol{r}_j, \quad \boldsymbol{r}_i = \sum_{j=1}^N (U^{-1})_{ij} \boldsymbol{x}_j. \quad (3.4)$$

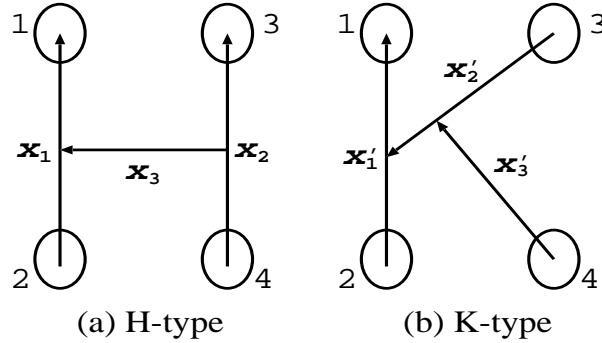


Figure 1. Relative coordinates for the four-body system

We use a matrix notation as much as possible in order to simplify formulas and expressions. Let \boldsymbol{x} denote an $(N-1)$ -dimensional column vector comprising all \boldsymbol{x}_i but the center of mass coordinate \boldsymbol{x}_N . Its transpose is a row vector and it is expressed as

$$\tilde{\boldsymbol{x}} = (\boldsymbol{x}_1, \boldsymbol{x}_2, \dots, \boldsymbol{x}_{N-1}). \quad (3.5)$$

The choice for \boldsymbol{x} is not unique but a set of Jacobi coordinates is conveniently employed. For the four-body system, the Jacobi set is identical to the K-type coordinate, and the corresponding matrix U is given by

$$U_K = \begin{pmatrix} 1 & -1 & 0 & 0 \\ \frac{1}{2} & \frac{1}{2} & -1 & 0 \\ \frac{1}{3} & \frac{1}{3} & \frac{1}{3} & -1 \\ \frac{1}{4} & \frac{1}{4} & \frac{1}{4} & \frac{1}{4} \end{pmatrix}. \quad (3.6)$$

The transformation matrix for the H-type coordinate reads

$$U_H = \begin{pmatrix} 1 & -1 & 0 & 0 \\ 0 & 0 & 1 & -1 \\ \frac{1}{2} & \frac{1}{2} & -\frac{1}{2} & -\frac{1}{2} \\ \frac{1}{4} & \frac{1}{4} & \frac{1}{4} & \frac{1}{4} \end{pmatrix}. \quad (3.7)$$

The K-type coordinate is obtained directly from the H-type coordinate by a transformation matrix $U_K U_H^{-1}$

$$U_K U_H^{-1} = \begin{pmatrix} 1 & 0 & 0 & 0 \\ 0 & -\frac{1}{2} & 1 & 0 \\ 0 & \frac{2}{3} & \frac{2}{3} & 0 \\ 0 & 0 & 0 & 1 \end{pmatrix} = \begin{pmatrix} U_{KH} & 0 \\ 0 & 1 \end{pmatrix}, \quad (3.8)$$

where U_{KH} is a 3×3 sub-matrix of $U_K U_H^{-1}$.

Each coordinate set emphasizes particular correlations among the nucleons. As mentioned above, the H-coordinate is natural to describe the $d+d$ channel, whereas the K-coordinate is suited for a description of the $3N+N$ partition. It is of crucial importance to include both types of motion in order to fully

describe the four-nucleon dynamics [2]. In order to develop a unified method that can incorporate both types of coordinates on an equal footing, we extend the explicitly correlated Gaussian function [37, 7] to include triple global vectors

$$\begin{aligned} & F_{L_1 L_2 (L_{12}) L_3 L M}(u_1, u_2, u_3, A, \mathbf{x}) \\ &= \exp\left(-\frac{1}{2}\tilde{\mathbf{x}}A\mathbf{x}\right) [[\mathcal{Y}_{L_1}(\tilde{u}_1\mathbf{x})\mathcal{Y}_{L_2}(\tilde{u}_2\mathbf{x})]_{L_{12}}\mathcal{Y}_{L_3}(\tilde{u}_3\mathbf{x})]_{LM}, \end{aligned} \quad (3.9)$$

where

$$\mathcal{Y}_{L_i M_i}(\tilde{u}_i\mathbf{x}) = |\tilde{u}_i\mathbf{x}|^{L_i} Y_{L_i M_i}(\widehat{\tilde{u}_i\mathbf{x}}) \quad (3.10)$$

is a solid spherical harmonics and its argument, $\tilde{u}_i\mathbf{x}$, what we call a global vector, is a vector defined through an $(N-1)$ -dimensional column vector u_i and \mathbf{x} as

$$\tilde{u}_i\mathbf{x} = \sum_{j=1}^{N-1} (u_i)_j \mathbf{x}_j, \quad (3.11)$$

where $(u_i)_j$ is the j th element of u_i . In Eq. (3.9) A is an $(N-1) \times (N-1)$ real and symmetric matrix, and it must be positive-definite for the function F to have a finite norm, but otherwise may be arbitrary. Non-diagonal elements of A can be nonzero.

The matrix A and the vectors u_1, u_2, u_3 are parameters to characterize the ‘‘shape’’ of the correlated Gaussian function. The Gaussian function including A describes a spherical motion of the system, while the global vectors are responsible for a rotational motion. The spatial function (3.3) is found to reduce to the general form (3.9). Suppose that \mathbf{x} stands for the H-type coordinate. Then a choice of $\tilde{u}_1=(1,0,0)$, $\tilde{u}_2=(0,1,0)$ and $\tilde{u}_3=(0,0,1)$ together with a diagonal matrix A provides us with the basis function (3.3) employed to represent the configurations of the $2N+2N$ channel. On the other hand, the K-type basis function looks like

$$\exp\left(-\frac{1}{2}\tilde{\mathbf{x}}'A_K\mathbf{x}'\right) [[\mathcal{Y}_{L_1}(\mathbf{x}'_1)\mathcal{Y}_{L_2}(\mathbf{x}'_2)]_{L_{12}}\mathcal{Y}_{L_3}(\mathbf{x}'_3)]_{LM}, \quad (3.12)$$

where $\tilde{\mathbf{x}}' = (\mathbf{x}'_1, \mathbf{x}'_2, \mathbf{x}'_3)$ is the K-coordinate set (see Fig. 1(b)) and A_K is a 3×3 diagonal matrix. Noting that \mathbf{x}' is equal to $\mathbf{x}' = U_{KH}\mathbf{x}$, we observe that the basis function (3.12) is obtained from Eq. (3.9) by a particular choice of parameters, that is, $\tilde{u}_1=(1,0,0)$, $\tilde{u}_2=(0,-\frac{1}{2},1)$ and $\tilde{u}_3=(0,\frac{2}{3},\frac{2}{3})$, and the matrix A is related to A_K by

$$A = (\tilde{u}_1\tilde{u}_2\tilde{u}_3)A_K \begin{pmatrix} \tilde{u}_1 \\ \tilde{u}_2 \\ \tilde{u}_3 \end{pmatrix} = \widetilde{U_{KH}}A_K U_{KH}. \quad (3.13)$$

Thus the form of the F -function remains unchanged under the transformation of relative coordinates.

Note that A is no longer diagonal. The choice of a different set of coordinates ends up only choosing appropriate parameters for A , u_1 , u_2 , and u_3 .

It is also noted that the triple global vectors in Eq. (3.9) are a minimum number of vectors to provide all possible spatial functions with arbitrary L and parity π . A natural parity state with $\pi = (-1)^L$ can be described by only one global vector, that is, using e.g., $L_1 = L$, $L_2 = 0$, $L_{12} = L$, $L_3 = 0$ [6, 38, 8]. To describe an unnatural parity state with $\pi = (-1)^{L+1}$ except for 0^- case, we need at least two global vectors, say, $L_1 = L$, $L_2 = 1$, $L_{12} = L$, $L_3 = 0$ [37, 7]. The simplest choice for the 0^- state is to use three global vectors with $L_1 = L_2 = L_{12} = L_3 = 1$ [37]. In this way, the basis function (3.9) can be versatile enough to describe bound states of not only four- but also more-particle systems with arbitrary L and π .

To assure the permutation symmetry of the wave function, we have to operate a permutation P on F . Since P induces a linear transformation of the coordinate set, a new set of the permuted coordinates, \mathbf{x}_P , is related to the original coordinate set \mathbf{x} as $\mathbf{x}_P = \mathcal{P}\mathbf{x}$ with an $(N-1) \times (N-1)$ matrix \mathcal{P} . As before, this permutation does not change the form of the F -function:

$$\begin{aligned} & PF_{L_1 L_2 (L_{12}) L_3 LM}(u_1, u_2, u_3, A, \mathbf{x}) \\ &= F_{L_1 L_2 (L_{12}) L_3 LM}(u_1, u_2, u_3, A, \mathbf{x}_P) \\ &= F_{L_1 L_2 (L_{12}) L_3 LM}(\tilde{\mathcal{P}}u_1, \tilde{\mathcal{P}}u_2, \tilde{\mathcal{P}}u_3, \tilde{\mathcal{P}}A\mathcal{P}, \mathbf{x}). \end{aligned} \quad (3.14)$$

The fact that the functional form of F remains unchanged under the permutation as well as the transformation of coordinates enables one to unify the method of calculating the matrix elements. This unique property is one of the most notable points in the present method.

4 Calculation of matrix elements

Calculations of matrix elements with the correlated Gaussian F are greatly facilitated with the aid of the generating function g [6, 5]

$$g(\mathbf{s}; A, \mathbf{x}) = \exp\left(-\frac{1}{2}\tilde{\mathbf{x}}A\mathbf{x} + \tilde{\mathbf{s}}\mathbf{x}\right), \quad (4.1)$$

with $\tilde{\mathbf{s}} = (\mathbf{s}_1, \mathbf{s}_2, \dots, \mathbf{s}_{N-1})$, where $\mathbf{s}_i = \sum_{j=1}^3 \lambda_j(u_j)_i \mathbf{e}_j$, \mathbf{e}_j is a 3-dimensional unit vector ($\mathbf{e}_j \cdot \mathbf{e}_j = 1$), and λ_j is a scalar parameter. More explicitly

$$\tilde{\mathbf{s}}\mathbf{x} = \sum_{i=1}^{N-1} \mathbf{s}_i \cdot \mathbf{x}_i = \sum_{i=1}^{N-1} \sum_{j=1}^3 \lambda_j(u_j)_i \mathbf{e}_j \cdot \mathbf{x}_i = \sum_{j=1}^3 \lambda_j \mathbf{e}_j \cdot (\tilde{u}_j \mathbf{x}). \quad (4.2)$$

The correlated Gaussian F is generated as follows:

$$\begin{aligned} & F_{L_1 L_2 (L_{12}) L_3 LM}(u_1, u_2, u_3, A, \mathbf{x}) \\ &= \left(\prod_{i=1}^3 \frac{B_{L_i}}{L_i!} \int d\mathbf{e}_i \right) [[Y_{L_1}(\mathbf{e}_1) Y_{L_2}(\mathbf{e}_2)]_{L_{12}} Y_{L_3}(\mathbf{e}_3)]_{LM} \\ &\times \left(\frac{\partial^{L_1+L_2+L_3}}{\partial \lambda_1^{L_1} \partial \lambda_2^{L_2} \partial \lambda_3^{L_3}} g(\mathbf{s}; A, \mathbf{x}) \right) \Bigg|_{\lambda_1=\lambda_2=\lambda_3=0}, \end{aligned} \quad (4.3)$$

where

$$B_L = \frac{(2L+1)!!}{4\pi}. \quad (4.4)$$

When $g(\mathbf{s}; A, \mathbf{x})$ is expanded in powers of λ_1 , only the term of degree $\lambda_1^{L_1}$ contributes in Eq. (4.3), and this term contains the L_1 th degree \mathbf{e}_1 because λ_1 and \mathbf{e}_1 always appear simultaneously. In order for the term to contribute to the integration over \mathbf{e}_1 , these L_1 vectors \mathbf{e}_1 must couple to the angular momentum L_1 because of the orthonormality of the spherical harmonics $Y_{L_1 M_1}(\mathbf{e}_1)$, that is, they are uniquely coupled to the maximum possible angular momentum. The same rule applies to λ_2, \mathbf{e}_2 and λ_3, \mathbf{e}_3 as well.

We outline a method of calculating the matrix element for an operator \mathcal{O}

$$\langle F_{L_4 L_5 (L_{45}) L_6 L' M'}(u_4, u_5, u_6, A', \mathbf{x}) | \mathcal{O} | F_{L_1 L_2 (L_{12}) L_3 L M}(u_1, u_2, u_3, A, \mathbf{x}) \rangle. \quad (4.5)$$

In what follows this matrix element is abbreviated as $\langle F' | \mathcal{O} | F \rangle$. Using Eq. (4.3) in Eq. (4.5) enables one to relate the matrix element to that between the generating functions:

$$\begin{aligned} \langle F' | \mathcal{O} | F \rangle &= \left(\prod_{i=1}^6 \frac{B_{L_i}}{L_i!} \int d\mathbf{e}_i \right) [[Y_{L_4}(\mathbf{e}_4) Y_{L_5}(\mathbf{e}_5)]_{L_{45}} Y_{L_6}(\mathbf{e}_6)]_{L' M'}^* \\ &\times [[Y_{L_1}(\mathbf{e}_1) Y_{L_2}(\mathbf{e}_2)]_{L_{12}} Y_{L_3}(\mathbf{e}_3)]_{L M} \\ &\times \left(\prod_{i=1}^6 \frac{\partial^{L_i}}{\partial \lambda_i^{L_i}} \right) \langle g(\mathbf{s}', A', \mathbf{x}') | \mathcal{O} | g(\mathbf{s}, A, \mathbf{x}) \rangle \Big|_{\lambda_i=0}, \end{aligned} \quad (4.6)$$

with

$$\mathbf{s} = \lambda_1 u_1 \mathbf{e}_1 + \lambda_2 u_2 \mathbf{e}_2 + \lambda_3 u_3 \mathbf{e}_3, \quad \mathbf{s}' = \lambda_4 u_4 \mathbf{e}_4 + \lambda_5 u_5 \mathbf{e}_5 + \lambda_6 u_6 \mathbf{e}_6. \quad (4.7)$$

The calculation of the matrix element consists of three stages: (1) Evaluate the matrix element between the generating functions, $\langle g(\mathbf{s}', A', \mathbf{x}') | \mathcal{O} | g(\mathbf{s}, A, \mathbf{x}) \rangle$. (2) Expand that matrix element in powers of λ_i and keep only those terms of degree L_i for each i . (3) Recouple the vectors \mathbf{e}_i and integrate over the angle coordinates. In the second stage the remaining terms should contain \mathbf{e}_i s of degree L_i as well. Hence any term with $\lambda_i^2 \mathbf{e}_i \cdot \mathbf{e}_i = \lambda_i^2$ etc. can be omitted because the degree of \mathbf{e}_i becomes smaller than that of λ_i .

We will explain the above procedures for the case of an overlap matrix element. The matrix element between the generating functions is

$$\langle g(\mathbf{s}', A', \mathbf{x}') | g(\mathbf{s}, A, \mathbf{x}) \rangle = \left(\frac{(2\pi)^{N-1}}{\det B} \right)^{3/2} \exp \left(\frac{1}{2} \tilde{\mathbf{z}} B^{-1} \mathbf{z} \right) \quad (4.8)$$

with

$$B = A' + A, \quad \mathbf{z} = \mathbf{s} + \mathbf{s}' = \sum_{i=1}^6 \lambda_i \mathbf{e}_i u_i. \quad (4.9)$$

To perform the operation in the second stage we note that

$$\frac{1}{2} \tilde{\mathbf{z}} B^{-1} \mathbf{z} = \frac{1}{2} \sum_{i,j=1}^6 \rho_{ij} \lambda_i \lambda_j \mathbf{e}_i \cdot \mathbf{e}_j \quad (4.10)$$

with

$$\rho_{ij} = \tilde{u}_i B^{-1} u_j. \quad (4.11)$$

As mentioned above, here we can drop the diagonal terms, $\lambda_i^2 \mathbf{e}_i \cdot \mathbf{e}_i$, and we get

$$\begin{aligned} & \left(\prod_{i=1}^6 \frac{\partial^{L_i}}{\partial \lambda_i^{L_i}} \right) \langle g(\mathbf{s}', A', \mathbf{x}') | g(\mathbf{s}, A, \mathbf{x}) \rangle \Big|_{\lambda_i=0} \\ &= \left(\frac{(2\pi)^{N-1}}{\det B} \right)^{3/2} \prod_{i=1}^6 L_i! \prod_{i<j}^6 \frac{(\rho_{ij} \mathbf{e}_i \cdot \mathbf{e}_j)^{n_{ij}}}{n_{ij}!}. \end{aligned} \quad (4.12)$$

Here the non-negative integers n_{ij} must satisfy the following equations in order to assure the degree L_i for \mathbf{e}_i in the different terms,

$$\begin{aligned} n_{12} + n_{13} + n_{14} + n_{15} + n_{16} &= L_1, \\ n_{12} + n_{23} + n_{24} + n_{25} + n_{26} &= L_2, \\ n_{13} + n_{23} + n_{34} + n_{35} + n_{36} &= L_3, \\ n_{14} + n_{24} + n_{34} + n_{45} + n_{46} &= L_4, \\ n_{15} + n_{25} + n_{35} + n_{45} + n_{56} &= L_5, \\ n_{16} + n_{26} + n_{36} + n_{46} + n_{56} &= L_6. \end{aligned} \quad (4.13)$$

The last step is to recouple the angular momenta arising from the various terms. Since we have to couple \mathbf{e}_i s to the angular momentum L_i from the terms of degree L_i , we may replace the term $(\rho_{ij} \mathbf{e}_i \cdot \mathbf{e}_j)^{n_{ij}}$ with just one piece

$$\frac{(-\rho_{ij})^{n_{ij}} n_{ij}! \sqrt{2n_{ij} + 1}}{B_{n_{ij}}} [Y_{n_{ij}}(\mathbf{e}_i) Y_{n_{ij}}(\mathbf{e}_j)]_{00}. \quad (4.14)$$

Other pieces like $[Y_\kappa(\mathbf{e}_i) Y_\kappa(\mathbf{e}_j)]_{00}$ with $\kappa < n_{ij}$ do not contribute to the matrix element. We thus have a product of 15 terms of $[Y_{n_{ij}}(\mathbf{e}_i) Y_{n_{ij}}(\mathbf{e}_j)]_{00}$. The coupling of these terms is done by defining various coefficients that are all expressed in terms of Clebsch-Gordan, Racah, and 9j coefficients. For example, we make use of the formulas

$$\begin{aligned} & [Y_a(\mathbf{e}_1) Y_a(\mathbf{e}_2)]_{00} [Y_b(\mathbf{e}_1) Y_b(\mathbf{e}_3)]_{00} [Y_c(\mathbf{e}_2) Y_c(\mathbf{e}_3)]_{00} \\ & \rightarrow X(abc) [[Y_{a+b}(\mathbf{e}_1) Y_{a+c}(\mathbf{e}_2)]_{b+c} Y_{b+c}(\mathbf{e}_3)]_{00}, \end{aligned} \quad (4.15)$$

$$\begin{aligned} & [Y_a(\mathbf{e}_1) Y_a(\mathbf{e}_4)]_{00} [Y_b(\mathbf{e}_1) Y_b(\mathbf{e}_5)]_{00} [Y_c(\mathbf{e}_1) Y_c(\mathbf{e}_6)]_{00} \\ & \rightarrow R_3(abc) [Y_{a+b+c}(\mathbf{e}_1) [[Y_a(\mathbf{e}_4) Y_b(\mathbf{e}_5)]_{a+b} Y_c(\mathbf{e}_6)]_{a+b+c}]_{00}. \end{aligned} \quad (4.16)$$

Here the symbol \rightarrow indicates that no other terms arising from the left hand side of the equation contribute to the integration over the angles \mathbf{e}_i s, so that only the

term on the right hand side has to be retained. Another coefficient is

$$\begin{aligned} & [[Y_a(\mathbf{e}_4)Y_b(\mathbf{e}_5)]_q Y_c(\mathbf{e}_6)]_Q [[Y_{a'}(\mathbf{e}_4)Y_{b'}(\mathbf{e}_5)]_{q'} Y_{c'}(\mathbf{e}_6)]_{Q'}]_\ell \\ & \rightarrow \sum_{\ell'} W(abcqQ, a'b'c'q'Q', \ell\ell') [[Y_{a+a'}(\mathbf{e}_4)Y_{b+b'}(\mathbf{e}_5)]_{\ell'} Y_{c+c'}(\mathbf{e}_6)]_\ell. \end{aligned} \quad (4.17)$$

Expressions for the coefficients, X, R_3, W , are given in Appendix A. Performing the integration of the six unit vectors, \mathbf{e}_i s, as prescribed in Eq. (4.6) leads to the overlap matrix element

$$\begin{aligned} & \langle F'|F \rangle \\ & = \left(\frac{(2\pi)^{N-1}}{\det B} \right)^{3/2} \left(\prod_{i=1}^6 B_{L_i} \right) \frac{(-1)^{L_1+L_2+L_3}}{\sqrt{2L+1}} \delta_{LL'} \delta_{MM'} \\ & \times \sum_{n_{ij}} \left(\prod_{i<j}^6 (-\rho_{ij})^{n_{ij}} \frac{\sqrt{2n_{ij}+1}}{B_{n_{ij}}} \right) O(n_{ij}; L_1 L_2 L_3 L_4 L_5 L_6, L_{12} L_{45} L), \end{aligned} \quad (4.18)$$

with

$$\begin{aligned} & O(n_{ij}; L_1 L_2 L_3 L_4 L_5 L_6, L_{12} L_{45} L) \\ & = X(n_{12} n_{13} n_{23}) R_3(n_{14} n_{15} n_{16}) R_3(n_{24} n_{25} n_{26}) R_3(n_{34} n_{35} n_{36}) X(n_{45} n_{46} n_{56}) \\ & \times Z(n_{12}+n_{13} \ L_1-n_{12}-n_{13}) Z(n_{12}+n_{23} \ L_2-n_{12}-n_{23}) Z(n_{13}+n_{23} \ L_3-n_{13}-n_{23}) \\ & \times \sum_{\ell_1 \ell_2 \ell_3} \begin{bmatrix} L_1 & L_1-n_{12}-n_{13} & n_{12}+n_{13} \\ L_2 & L_2-n_{12}-n_{23} & n_{12}+n_{23} \\ L_{12} & \ell_1 & n_{13}+n_{23} \end{bmatrix} \begin{bmatrix} L_{12} & \ell_1 & n_{13}+n_{23} \\ L_3 & L_3-n_{13}-n_{23} & n_{13}+n_{23} \\ L & L & 0 \end{bmatrix} \\ & \times W(n_{14} n_{15} n_{16} \ n_{14}+n_{15} \ L_1-n_{12}-n_{13}, n_{24} n_{25} n_{26} \ n_{24}+n_{25} \ L_2-n_{12}-n_{23}, \ell_1 \ell_2) \\ & \times W(n_{14}+n_{24} \ n_{15}+n_{25} \ n_{16}+n_{26} \ \ell_2 \ \ell_1, n_{34} n_{35} n_{36} \ n_{34}+n_{35} \ L_3-n_{13}-n_{23}, L \ell_3) \\ & \times W(L_4-n_{45}-n_{46} \ L_5-n_{45}-n_{56} \ L_6-n_{46}-n_{56} \ \ell_3 \ L, \\ & \quad n_{45}+n_{46} \ n_{45}+n_{56} \ n_{46}+n_{56} \ n_{46}+n_{56} \ 0, LL_{45}), \end{aligned} \quad (4.19)$$

where Z is the coefficient given in Eq. (A.3). The summation in Eq. (4.18) extends over all possible sets of n_{ij} that satisfy Eq. (4.13). In most cases the values of L_i are limited up to 2, so that the number of terms to be evaluated is not so large and the calculation of the matrix element is fast.

Expressions for the Hamiltonian matrix elements are collected in Appendix B. One advantage of our method is that the calculation of matrix elements can be done analytically. In addition we do not need to do angular momentum and parity projections because the correlated Gaussian function (3.9) already preserves those quantum numbers.

The Fourier transform of the correlated Gaussian function F is a momentum space function and it becomes a useful tool to calculate various matrix elements that depend on the momentum operators [7]. For example, the distribution of the relative momentum is obtained by the expectation value of $\delta(\mathbf{p}_i - \mathbf{p}_j - \mathbf{p})$, where \mathbf{p}_j is the momentum of the j th particle. It is obviously much easier to calculate the distribution using the momentum space function rather than the coordinate space function. We show in Appendix C that the Fourier transform of F reduces to a linear combination of F s in the momentum space.

5 Results

5.1 $2N+2N$ and $3N+N$ channels

In Table 1, we gave the physical channels, $d+d$, $t+p$, and $h+n$. Fig. 2 displays two-body decay thresholds in the $d+d$ threshold energy region. The three physical channels are the main channels that describe the scattering around the three lowest thresholds ($d+d$, $t+p$, $h+n$). However, the scattering wave function $\Psi_{\text{int}}^{JM\pi}$ in the internal region should contain all effects that may occur when all the nucleons come close to each other. It is thus reasonable that $\Psi_{\text{int}}^{JM\pi}$ may not be well described in terms of the physical channels alone. Particularly the deuteron can be easily distorted when we use realistic potentials.

We will show that some pseudo $2N+2N$ channels are indeed needed to simulate the distortion of the deuteron. These pseudo channels, when they are included in the phase-shift calculation, are expected to take account of the distortion of the clusters of the entrance channel [30]. Here “pseudo” means that the clusters in the pseudo channels are not physically observable but may play a significant role in the internal region. The wave functions of these $2N$ pseudo clusters are obtained by diagonalizing the intrinsic cluster Hamiltonian similarly to the case of the physical clusters. We take into account the following pseudo clusters: $d^*(1^+, T=0)$, $d^*(0^+, T=1)$, $d^*(2^+, T=0)$, $d^*(3^+, T=0)$, $2n^*(0^+, T=1)$, and $2p^*(0^+, T=1)$, where the upper suffix * indicates all the excited state but the ground state of d . Among the pseudo clusters, the lowest energy states with 0^+ that are related to virtual states would be most im-

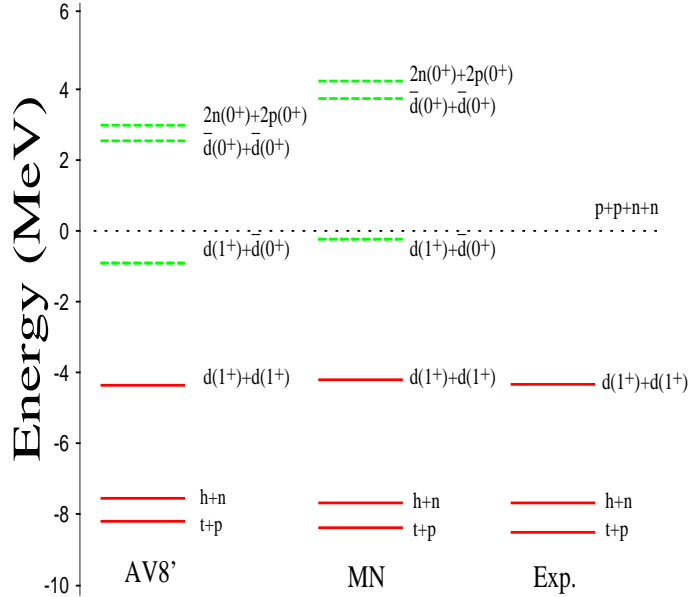


Figure 2. Two-body thresholds calculated with the AV8' (left) and MN (middle) potentials. The solid lines are physical channels and the dashed lines are pseudo channels. We also plot experimental two-body thresholds for physical channels (right). The dotted line is the $p+p+n+n$ threshold.

Table 3. $2N+2N$ and $3N+N$ channels. The Roman and Arabic numerals correspond to sets of channels included in the calculations.

model		channel	
FULL	$2N+2N$	I	$d(1^+)+d(1^+)$
			$d(1^+)+d^*(1^+)$
			$d^*(1^+)+d^*(1^+)$
		II	$\bar{d}(0^+)+\bar{d}(0^+)$
			$\bar{d}(0^+)+d^*(0^+)$
			$d^*(0^+)+d^*(0^+)$
		III	$d^*(2^+)+d^*(1^+)$
			$d^*(2^+)+d^*(2^+)$
		IV	$d^*(3^+)+d^*(1^+)$
			$d^*(3^+)+d^*(2^+)$
	$d^*(3^+)+d^*(3^+)$		
	V	$2n(0^+)+2p(0^+)$	
		$2n(0^+)+2p^*(0^+)$	
		$2n^*(0^+)+2p(0^+)$	
$2n^*(0^+)+2p^*(0^+)$			
$3N+N$	1	$t(\frac{1}{2}^+)+p(\frac{1}{2}^+)$	
		$t^*(\frac{1}{2}^+)+p(\frac{1}{2}^+)$	
	2	$h(\frac{1}{2}^+)+n(\frac{1}{2}^+)$	
		$h^*(\frac{1}{2}^+)+n(\frac{1}{2}^+)$	

portant. We especially write them as $\bar{d}(0^+)$, $2n(0^+)$ (di-neutron) and $2p(0^+)$ (di-proton). Although they are not bound, they are observed as resonances or quasi-bound states with negative scattering lengths. In fact the scattering lengths are $a_s(nn) = -16.5$ fm and $a_s(pp) = -17.9$ fm, which are comparable to $a_s(np, T = 1) = -23.7$ fm. The calculated thresholds of these pseudo channels are also drawn in Fig. 2.

Though it is expected that the pseudo channels with low threshold energies contribute more strongly to the scattering phase shift, we take into account all of these $2N+2N$ channels that include a vanishing total isospin as given in Fig. 2. The total isospin of the $3N+N$ channel is mixed in the present calculation. Because the $T=1$ component of the scattering wave function only weakly couples to the $d(1^+, T = 0)+d(1^+, T = 0)$ elastic-channel, the channel $d(1^+, T = 0)+\bar{d}(0^+, T = 1)$ is not employed in the calculation.

We also include the excited deuteron channels that comprise the $d^*(2^+, T = 0)$ and $d^*(3^+, T = 0)$ clusters. The energies of these lowest thresholds are above 10 MeV. These channels are therefore expected not to be very important, but that is not always the case as will be discussed in the case of the 1S_0 $d+d$ phase shift.

Table 3 summarizes all the channels that are used in our calculation. The $2N+2N$ channels are distinguished by Roman numerals, while the $3N+N$ chan-

nels are labeled by Arabic numerals. In the following, we use an abbreviation “ $2N+2N$ ” or “ $3N+N$ ” to indicate calculations including all $2N+2N$ channels I-V or all $3N+N$ channels (1-2 in Table 3), respectively. Here $t^*(\frac{1}{2}^+)$ and $h^*(\frac{1}{2}^+)$ are excited $3N$ continuum states. A “FULL” calculation indicates that all the channels in the table are included to set up the S -matrix. In the case of the MN potential channels III and IV are not included because this potential contains no tensor force.

The relative wave functions $\chi_{\alpha m}$ are expanded with 15 basis functions. We checked the stability of the S -matrix against the choice of the channel radius. The channel radius employed in this calculation is about 15 fm.

5.2 Positive parity phase shifts

Fig. 3 displays the 1S_0 $d+d$ elastic-scattering phase shift obtained with the AV8' potential. The dash-dotted line is the phase shift calculated with channel I ($I_d = 1^+$), and the dash-dot-dotted line is the phase shift with channels I and II ($I_d = 1^+, 0^+$). The phase shifts calculated by including further excited deuterons are also plotted by the dashed and dotted lines that correspond to the channels I-III ($I_d \leq 2^+$) and I-IV ($I_d \leq 3^+$), respectively. A naive expectation that the 1S_0 $d+d$ elastic-scattering phase shift might be well described in channel I ($d(1^+) + d(1^+)$, $d(1^+) + d^*(1^+)$ and $d^*(1^+) + d^*(1^+)$) alone completely breaks down in the case of the AV8' potential.

Because the deuteron has a virtual state \bar{d} with 0^+ at low excitation energy, it is reasonable that the inclusion of channel II gives rise to a considerable attractive effect of several tens of degrees on the phase shift, as shown by the dash-dot-dotted line of Fig. 3. However, the phase shift exhibits no converging behavior even when the higher spin states such as $d^*(2^+)$ and $d^*(3^+)$ are taken into account in the calculation. The additional attractions by these channels are of the same

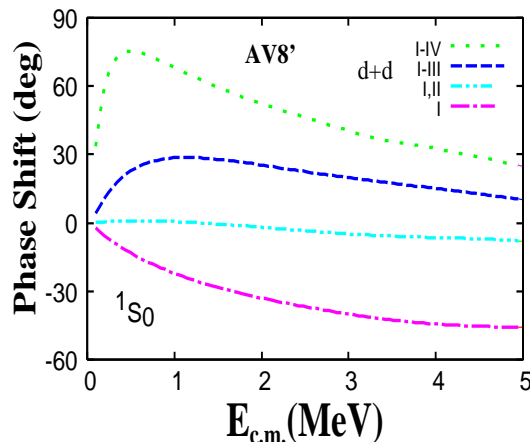


Figure 3. 1S_0 $d+d$ elastic-scattering phase shift calculated with the AV8' potential. The phase shifts are all obtained within the $d+d$ channels. The set of included channels is successively increased from I to IV. See Table 3 for the deuteron states included in each channel.

order as that of channel II. One may conclude that the deuteron is strongly distorted even in the low energy 1S_0 $d+d$ elastic scattering but more physically we have to realize that there exist two observed 0^+ states below the $d+d$ threshold. Obviously the $d+d$ scattering wave function is subject to the structure of those states in the internal region.

The second 0^+ state of ^4He lying about 4 MeV below the $d+d$ threshold is known to have a $3N+N$ cluster structure [39, 34]. Thus this state together with the ground state of ^4He cannot be described well in the $2N+2N$ model space alone. As seen in Table 1, the $3N+N$ channel contains a 1S_0 component, which is the dominant component of the 0_2^+ state. Since the realistic force strongly couples the $2N+2N$ channel to the $3N+N$ channel and the $d+d$ scattering wave function has to be orthogonal to the main component of the underlying 0^+ states, we expect that the deuteron in the incoming $d+d$ channel never remains in its ground state but has to be distorted largely due to the $3N+N$ channel. The phase shift for the channel I-IV (dotted line) shows a resonant pattern. This resonant state is expected to be the second 0^+ state because of the restricted model space within the $d+d$ channel.

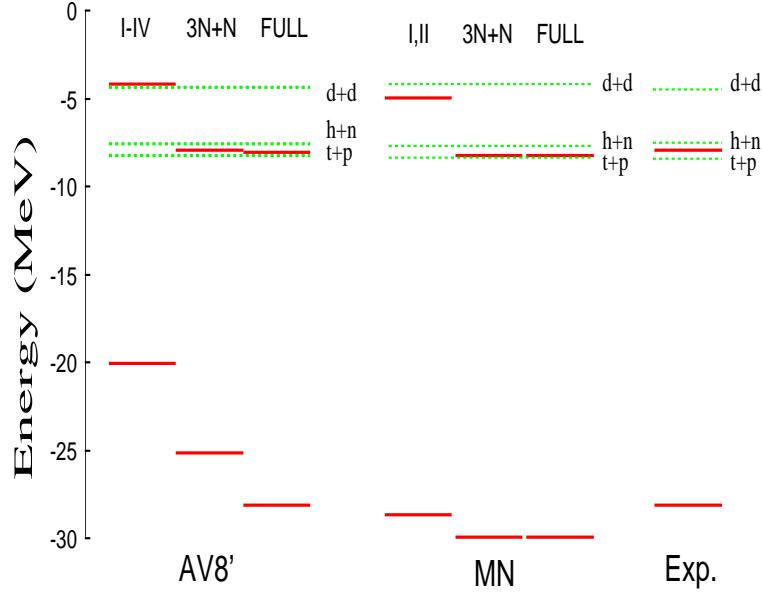


Figure 4. Comparison of the ground and second 0^+ state energies between calculations with the AV8' (left) and MN (middle) potentials and experiment (right). The model space for AV8' is I-IV, $3N+N$ and FULL and the model space for MN is I-II, $3N+N$ and FULL.

Fig. 4 displays the calculated ground state energy and the second 0^+ energy for the AV8' (left) and MN (middle) potentials. The model spaces of the calculations are I-IV, $3N+N$ and FULL for AV8' and I-II, $3N+N$ and FULL for MN. We also plot experimental energies (right) [40]. For the AV8' potential, the energies of the two lowest 0^+ states do not change very much between the FULL and $3N+N$ models. But the second 0^+ state with the $d+d$ model (channels I-IV) is not bound with respect to the $d+d$ threshold as expected before.

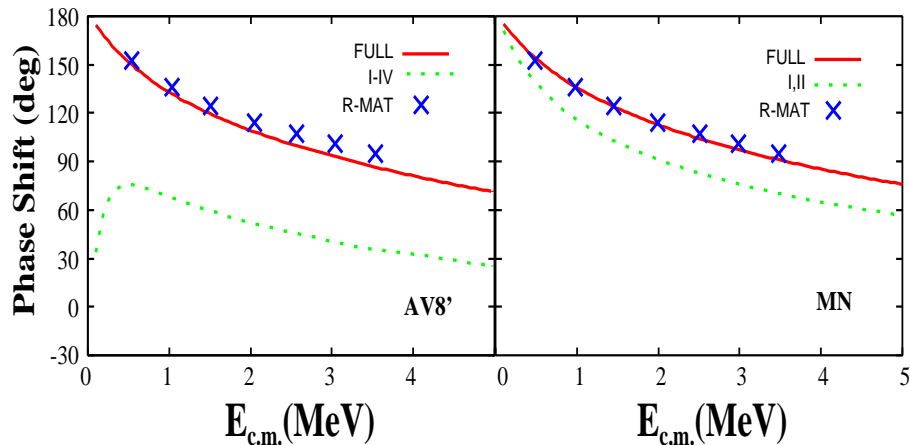


Figure 5. 1S_0 $d+d$ elastic-scattering phase shift calculated with the AV8' (left) and MN (right) potentials. The solid line is a FULL calculation, while the dotted line is a $d+d$ channel calculation. Crosses correspond to the R -matrix analysis of Ref. [22].

On the contrary, for the MN potential, the second 0^+ state with the $d+d$ model (channels I-II) is bound with respect to the $d+d$ threshold. We consider that this difference makes the drastic change of the $d+d$ phase shifts, between the AV8' and MN potentials. It is also interesting to see that the energies of the two lowest 0^+ states for the MN potential are almost the same between the FULL and $3N+N$ models.

Plotted in Fig. 5 are the 1S_0 $d+d$ elastic-scattering phase shifts obtained with the AV8' potential (left) and the MN potential (right). The FULL calculation (solid line) couples all $2N+2N$ and $3N+N$ channels that are listed in Table 3. The R -matrix analysis (crosses) [22] is reproduced well by both the AV8' and MN potential with the FULL calculation. Compared to the uncoupled phase shift (dotted line), one clearly sees that the $3N+N$ channel produces a very large effect on the $d+d$ elastic phase shift, especially in the case of the AV8' potential. We also verified that a calculation excluding the channels III, IV or V from the FULL channel calculation gives only negligible change in the phase shift. The slow convergence seen in Fig. 3 is thus attributed to the neglect of the $3N+N$ channel, indicating that a proper account of the 1S_0 $d+d$ elastic phase shift at low energy can be possible only when the coupled channels $\{d(1^+)+d(1^+)\} + \{d(0^+)+d(0^+)\} + \{t(1/2^+)+p(1/2^+)\} + \{h(1/2^+)+n(1/2^+)\}$ are considered.

Thus, the slow convergence in Fig. 3 suggests that the $2N+2N$ partition is not an economical way to include the effects of the $3N+N$ channel. In the case of the MN potential (right panel in Fig. 5), the situation is very different from the AV8' case. The channel coupling effect is rather modest, and the size of the 1S_0 $d+d$ elastic phase shift is already accounted for mostly in the $d+d$ channel calculation. All these results are very consistent with the 0^+ spectrum in Fig. 4.

The large distortion effect of the deuteron clusters on the 1S_0 $d+d$ scattering phase shift is expected to appear in the $3N+N$ phase shift as well because of the coupling between the $3N+N$ and $2N+2N$ channels. We display in Fig. 6

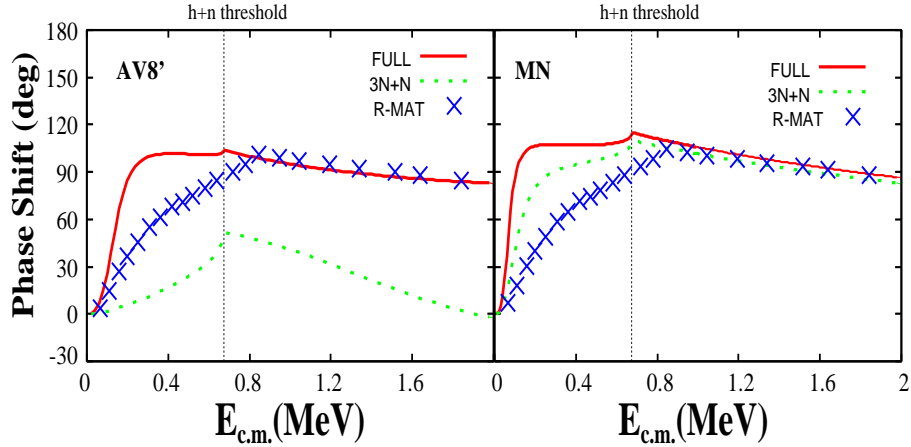


Figure 6. 1S_0 $t+p$ elastic-scattering phase shift at energies below the $d+d$ threshold. The solid line is a FULL calculation, while the dashed line is a $3N+N$ channel calculation. Crosses correspond to the R -matrix analysis of Ref. [22].

the 1S_0 $t+p$ elastic-scattering phase shift at energies below the $d+d$ threshold. The 0_2^+ state of ^4He is observed as a sharp resonance with a proton decay width of 0.5 MeV at about 0.4 MeV above the $t+p$ threshold. The present energies ($E_r = 0.15$ MeV for AV8', $E_r = 0.12$ MeV for MN) calculated with a bound state approximation are slightly smaller than the experimental value, but they are consistent with a calculation ($E_r = 0.105$ MeV and $\Gamma/2 = 0.129$ MeV for AV18+UIX, $E_r = 0.091$ MeV and $\Gamma/2 = 0.077$ MeV for AV18+UIX+ V_3^*) with another realistic interaction (AV18) with three nucleon forces by Hofmann and Hale [22]. The calculated phase shifts appear slightly larger than that in the R -matrix analysis (crosses in Fig. 6) [22]. It is noted that the phase shift changes so much even for a small change of the 0_2^+ resonant pole position (~ 0.1 MeV) because it is very near to the threshold. The phase shifts in the FULL calculation, for both AV8' and MN cases, show a resonance pattern in a small energy interval and the overall energy dependencies of the phase shifts are similar to each other. However, the phase shifts obtained only in the $3N+N$ channel are quite different as indicated by the dotted lines in Fig. 6. In the case of the MN potential (right) the phase shift is already close to the FULL phase shift, while in the case of the AV8' potential (left) the phase shift is much smaller (by almost 90 degrees) and moreover shows no resonance pattern.

By looking into the wave functions in more detail, we argue that the large distortion effect in the 1S_0 $d+d$ and $3N+N$ coupled channels is really brought about by the tensor force. As shown in Table 2, the AV8' potential with TNF gives 5.8% and 8.4% (8.3%) D -state probability for d and t (h), respectively. Thus the $d+d$ state in the 1S_0 state contains $L = S = 0$ components (89%) as well as $L = S = 2$ components (11%), where L and S are the total orbital and spin angular momenta of the four-nucleon system. Similarly the $3N+N$ state in the 1S_0 state contains an $L = S = 0$ component (92%) and an $L = S = 2$ component (8%). Thus the tensor force couples both states with $\Delta L = 2$ and

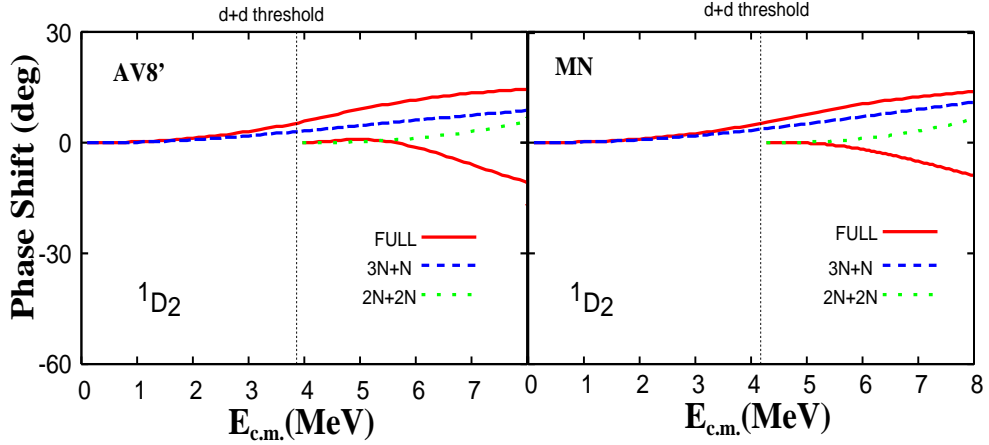


Figure 7. 1D_2 elastic-scattering phase shifts with the AV8' (left) and MN (right) potentials. The model space for the solid line is FULL. The $t+p$ phase shift starts from the $t+p$ zero energy and the $d+d$ phase shift starts from the $d+d$ threshold. The dashed line is the $t+p$ phase shift with only the $3N+N$ channel and the dotted line is the $d+d$ phase shift with only the $2N+2N$ channel.

$\Delta S = 2$ couplings, which are in fact very large compared to the central matrix element ($\Delta L = 0$, $\Delta S = 0$). An analysis of this type was performed for some levels of ^4He in Refs. [7, 39]. The MN potential contains no tensor force, so that the $d+d$ and $3N+N$ channel coupling is modest.

As listed in Table 1, there are four channels, 5S_2 , 1D_2 , 3D_2 and 5D_2 , for $J^\pi = 2^+$ at energies around the $d+d$ threshold. Among these states, we expect that the effect of the coupling between the $3N+N$ and $2N+2N$ channels occurs most strongly in 1D_2 as it appears in all physical channels. However, no sharp resonance is observed in ^4He up to 28 MeV of excitation energy, so that the coupling effect, if any, might be weaker than that observed in the 1S_0 case.

Fig. 7 displays the 1D_2 elastic-scattering phase shifts obtained in three types of calculations, $3N+N$ (dashed line), $2N+2N$ (dotted line), and FULL (solid line). The $t+p$ and $d+d$ phase shifts start from the $t+p$ ($E_{c.m.} = 0$) and $d+d$ thresholds, respectively. The phase shifts of the $3N+N$ and $2N+2N$ calculations are both slightly positive, indicating a weak attraction in the $t+p$ and $d+d$ interactions. In the FULL calculation, the $t+p$ phase shift becomes more attractive and the $d+d$ phase shift turns to be negative (repulsive). The present FULL calculation reproduces the calculation of Ref. [22] as expected. Though the effect of the coupling is slightly larger in the AV8' potential than in the MN potential, it is much less compared to the case of the 1S_0 phase shift. This is understood as follows. In the 1D_2 state, the main component of the wave function is given by the $L = 2$, $S = 0$ state: Its probability is the same as that of 1S_0 , that is, 92% in $t+p$ and 89% in $d+d$. However, the probability of finding the state with $L = 0$, $S = 2$, which causes a strong tensor coupling, is more than one order of magnitude smaller than in the case of 1S_0 , namely 0.23% in $t+p$ and 0.44% in $d+d$, respectively. The reason for this small percentage is that, to obtain $L = 0$, the incoming D -wave in the 1D_2 channel must couple with the D -components

in the clusters, but this coupling leads to several fragmented components with different L values. This relatively weaker coupling of the tensor force explains the phase shift behavior in Fig. 7.

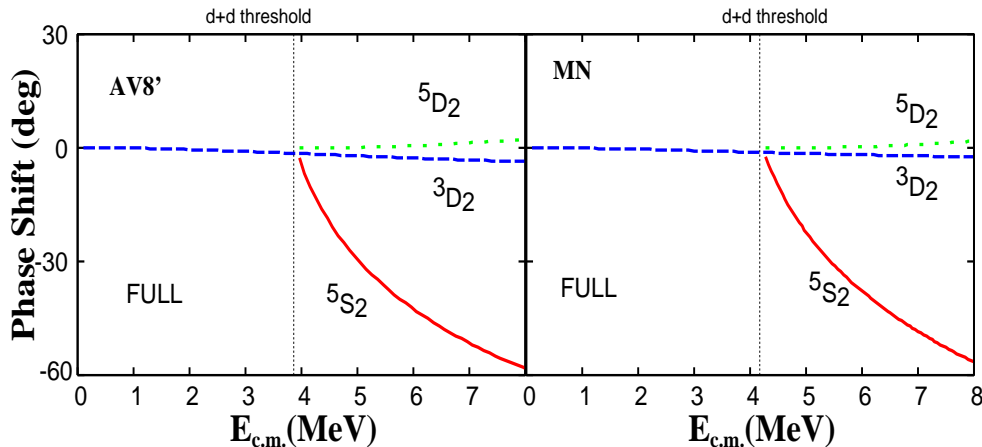


Figure 8. Elastic scattering phase shifts of the 2^+ state obtained in a FULL calculation with the AV8' (left) and MN (right) potentials. Solid line: 5S_2 $d+d$ phase shift, dotted line: 5D_2 $d+d$ phase shift, dashed line: 3D_2 $t+p$ phase shift.

In Fig. 8 we plot the $t+p$ and $d+d$ elastic-scattering phase shifts for other channels, 5S_2 (solid line), 3D_2 (dashed line), and 5D_2 (dotted line). We show only the FULL result, because the phase shifts with the truncated basis do not change visibly at the scale of the figure. The obtained phase shifts are not that different between the AV8' and MN potentials, and also consistent with the previous calculation [22]. Thus, the effect of the distortion of the clusters is very small for 2^+ except for 1D_2 .

We have three channels for $J^\pi = 1^+$, 5D_1 , 3D_1 and 3S_1 . No sharp 1^+ resonance of ${}^4\text{He}$ is observed experimentally up to 28 MeV of excitation energy. Another theoretical calculation neither predicts it [39], so that the coupling between the $2N+2N$ and $3N+N$ channels is expected to be weak. Fig. 9 exhibits the $t+p$ and $d+d$ elastic-scattering phase shifts in the FULL calculation: 5D_1 $d+d$ (solid line), 3D_1 $t+p$ (dashed line), and 3S_1 $t+p$ (dotted line). Only the FULL result is displayed because the phase shift change in other calculations is small. Both AV8' and MN potentials produce phase shifts quite similar to each other.

5.3 Negative parity phase shifts

As seen from Table 1, the main components of these negative parity states are considered to be 3P_J .

We compare in Fig. 10 the 3P_0 elastic-scattering phase shifts calculated with the AV8' (left) and MN (right) potentials. The truncated $3N+N$ (dashed line) and $2N+2N$ (dotted line) calculations are shown together with the FULL result (solid line). The $t+p$ phase shift of the $3N+N$ calculation is similar with both AV8' and MN potentials, while the $d+d$ phase shift of the $2N+2N$ calculation

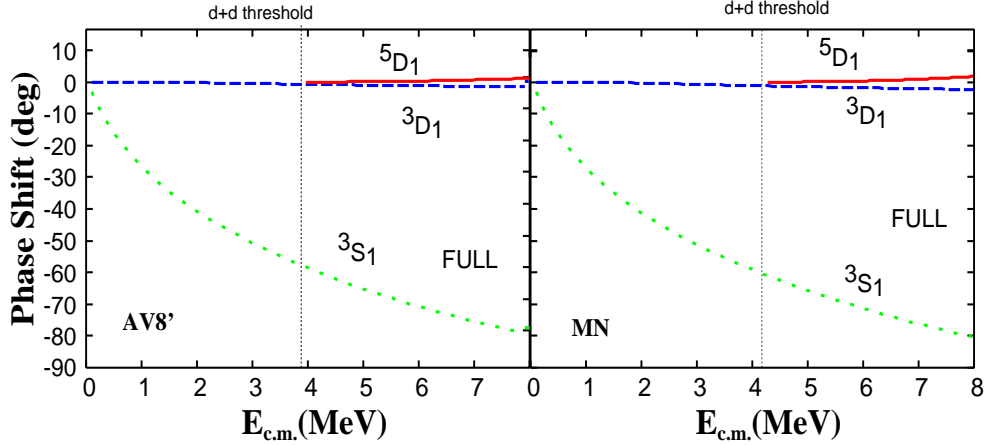


Figure 9. Elastic scattering phase shifts of the 1^+ state in a FULL calculation with the AV8' (left) and MN (right) potentials. Solid line: 5D_1 $d+d$ phase shift, dotted line: 3S_1 $t+p$ phase shift, dashed line: 3D_1 $t+p$ phase shift.

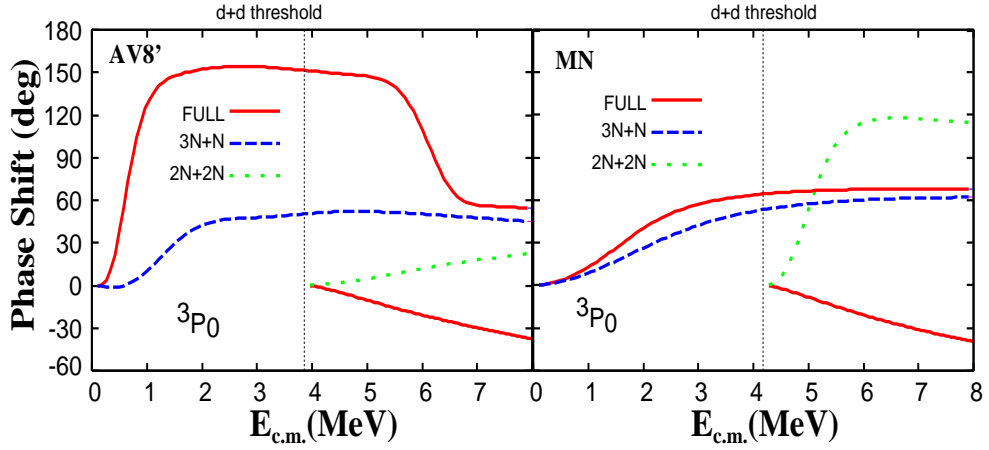


Figure 10. 3P_0 elastic-scattering phase shifts calculated with the AV8' (left) and MN (right) potentials. See the caption of Fig. 7.

tion behaves quite differently between the two potentials: the $d+d$ phase shift is weakly attractive with AV8' but is very strongly attractive with MN. No typical resonance behavior shows up below the $d+d$ threshold, which is in contradiction to experiment. In the FULL model that combines both $3N+N$ and $2N+2N$ configurations, however, the two potentials predict quite different phase shifts especially in the $t+p$ channel. The $t+p$ phase shift with AV8' becomes so attractive that it crosses $\pi/2$, indicating a resonance at about 1 MeV above the $t+p$ threshold. The $d+d$ phase shift changes sign from attractive to repulsive. The result based on the AV8' potential is thus consistent with experiment. Furthermore, we reproduce the flat structure of the 3P_0 phase shift around several MeV above the $t+p$ threshold which was discussed as the coupling to the $h+n$ channel [22]. On the other hand, the MN potential changes the $t+p$ phase shift only

mildly and produces no sharp resonance behavior. The $d+d$ phase shift changes drastically to the repulsive side.

As seen in the above figure, the sharp 0^- state appears provided a full model space with a realistic potential is employed. The mechanism to produce this resonance is unambiguously attributed to the tensor force as discussed in Ref. [7] for the realistic interaction G3RS [41]. According to it, the 0^- state consists of only two components, $L = S = 1$ (95.5%) and $L = S = 2$ (4.5%), ignoring a tiny component with $L = S = 0$. The $L = S = 2$ component arises from the coupling of the incoming P -wave with the D -states contained in the $3N$ and d clusters. All the pieces of the Hamiltonian but the tensor force have no coupling matrix element between the two components. The uncoupled Hamiltonian thus gives a too high energy to accommodate a resonance. The tensor force, however, couples the two components very strongly, bringing down its energy to a right position.

The second lowest negative parity state has spin-parity 2^- . The physical channel for this state is only 3P_2 as seen in Table 1. Fig. 11 compares the 3P_2 elastic-scattering phase shifts in a manner similar to Fig. 10. The phase shift obtained with the MN potential is almost the same as the 3P_0 phase shift, which is consistent with the previous result [39] that the energies of the negative parity states calculated with the MN potential are found to be degenerate. In the case of the AV8' potential, the 3P_2 phase shifts grows significantly in the FULL calculation, indicating a resonant behavior. The coupling effect between the $3N+N$ and $2N+2N$ channels is however much less compared to the 0^- state. This is because the incoming P -wave coupled to the D -states in the clusters gives rise to several L values to produce the 2^- state and therefore the tensor coupling does not concentrate sufficiently to produce a sharp resonance.

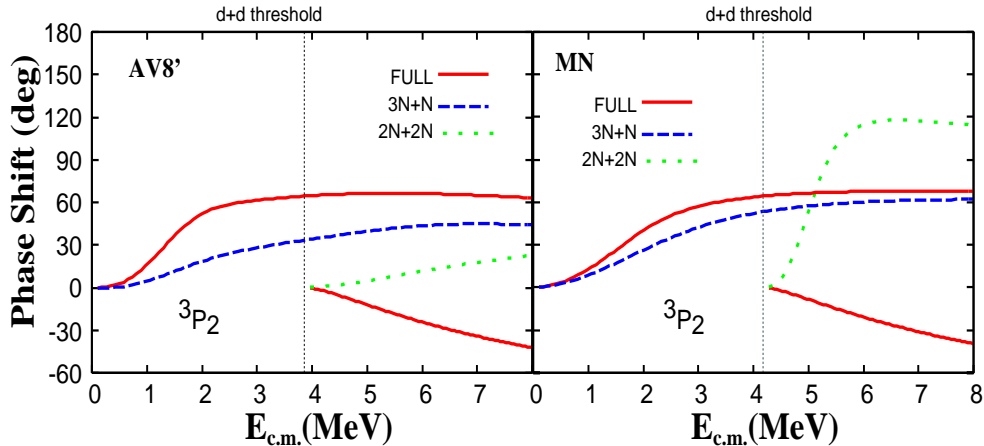


Figure 11. 3P_2 elastic-scattering phase shifts calculated with the AV8' (left) and MN (right) potentials. See the caption of Fig. 7.

Fig. 12 displays the 3P_1 and 1P_1 elastic-scattering phase shifts calculated with the AV8' (left) and MN (right) potentials. Note that no physical $d+d$ channel exists in the case of the 1P_1 state. Because both FULL and $3N+N$ calculations give almost the same phase shifts, only the FULL result is shown in the figure.

The 3P_1 phase shift calculated with the MN potential is again almost the same as those of the 3P_0 and 3P_2 cases, supporting that the three negative parity states become almost degenerate. The 3P_1 elastic-scattering phase shift calculated with the AV8' potential is qualitatively similar to that of 3P_2 . The attractive nature of the $t+p$ phase shift becomes further weaker, and to identify a resonance appears to be very hard. Even though it is possible in some way, its width would be a few MeV, which is not in contradiction to experiment. The 1P_1 phase shifts are very small in both AV8' and MN cases.

For the negative parity states, the FULL model with the AV8' potential gives results that are consistent with both experiment and the theoretical calculation of Ref. [39]. We have pointed out that the phase shift behavior reveals the importance of the tensor force particularly in the case of 0^- . Its effect is often masked however by the coupling between the D states in the clusters and the incoming partial wave.

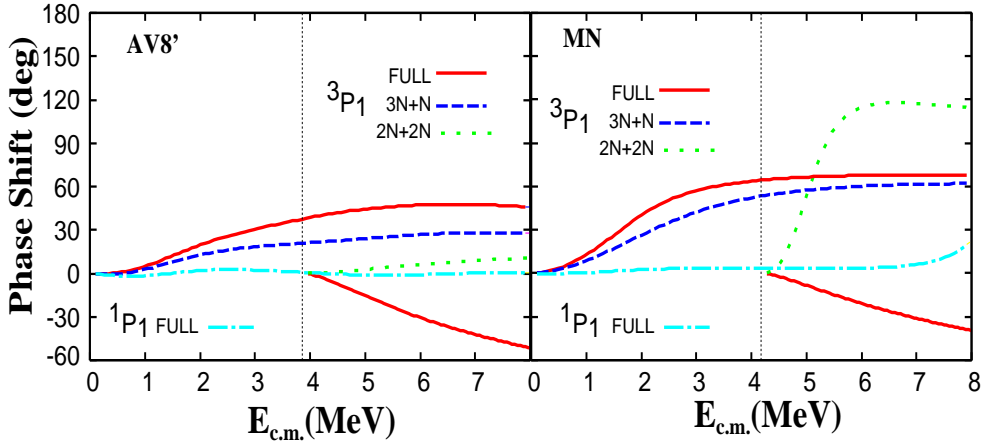


Figure 12. 3P_1 and 1P_1 elastic-scattering phase shifts calculated with the AV8' (left) and MN (right) potentials. See the caption of Fig. 7.

In this subsection, we investigate the phase shifts of the negative parity states which have dominant $T = 0$ components. In Fig. 13, we represent three experimental negative parity $T = 0$ energies (left). The states are observed at -7.29 (0^-), -6.46 (2^-) and -4.05 (1^-) MeV below the four-nucleon threshold [40]. The former two are located below the $d+d$ threshold and their widths are 0.84 and 2.01 MeV, respectively, whereas the last one is above the $d+d$ threshold and its width is fairly broad (6.1 MeV). Here, we calculate these energies as -7.57 (0^-), -6.82 (2^-) and -5.95 (1^-) MeV, which are approximated by the half-value position from the maximum phase shifts. The present calculation is not projected out to $T = 0$, but the dominant configurations of $t+p$, $h+n$ and $d+d$ elastic scattering are $T = 0$. Our calculated energies with AV8' reproduce the ordering of 0^- , 2^- and 1^- (middle in Fig. 13). The splitting between the two lower states 0^- and 2^- is reproduced, but the experimental 1^- energy is higher than the calculation. However, the determination of the energy for such a high energy state with large decay width (6.1 MeV) is very difficult from both experimental

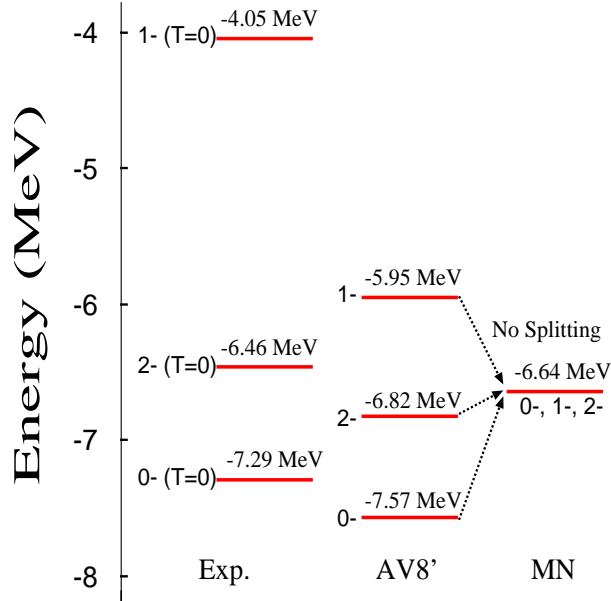


Figure 13. Comparison of energies with respect to the four-nucleon threshold for negative parity states (0^- , 1^- , 2^-) between the experiment (left), AV8' (middle) and MN (right).

and theoretical side, and it usually has a large ambiguity.

This type of analysis was done by Horiuchi and Suzuki, who applied the correlated Gaussian basis with two global vectors to study the energy spectrum of ${}^4\text{He}$ [39]. Because the results of Ref. [39] are based on approximate solutions that impose no proper resonance boundary condition, it is interesting to see how the tensor force changes the phase shifts in the negative parity states as shown in this subsection. These authors also found that the negative parity states with $T = 0$ turn out to be almost degenerate when the MN potential that contains no tensor force is employed. In the present calculation, three states (0^- , 1^- , 2^-) completely degenerate at the same energy, $E = -6.64$ MeV (right), and the same phase shift pattern (solid lines in Figs. 10, 11, 12). Thus we can expect to see a clear evidence for the tensor force in the scattering involving the negative parity states.

6 Summary and conclusion

We have investigated the distortion of clusters appearing in the low-energy $d+d$ and $t+p$ elastic scattering using a microscopic cluster model with the triple global vector method. We showed that the tensor interaction changes the phase shifts very much by comparing a realistic interaction and an effective interaction. In the present *ab-initio* type cluster model, the description of the cluster wave functions is extended from a simple ($0s$) harmonic-oscillator shell model to a few-body model. To compare distortion effects of the clusters with realistic and effective interactions, we employed the AV8' potential as a realistic interaction

and the MN potential as an effective interaction.

For the realistic interaction, the calculated 1S_0 phase shift shows that the $t+p$ and $h+n$ channels strongly couple with the $d+d$ channel. These channels are coupled because of the tensor interaction. On the contrary, the coupling of these $3N+N$ channels plays a relatively minor role for the case of the effective interaction because of the absence of tensor term. In other words, the $3N+N$ channels strongly affect the $d+d$ elastic phase shift with the realistic interaction, but not with the effective interaction.

For the 2^+ phase shifts, there is a 1D_2 component in all physical channels ($d+d$, $t+p$ and $h+n$). The coupling of the $2N+2N$ and $3N+N$ channels in 5D_2 is weaker than in 1S_2 because of a weaker tensor coupling as discussed in section 5, and the calculated phase shifts are very similar for the realistic and effective potentials. For other positive parity cases, the phase shift behavior of the realistic and effective potentials are very similar, and the coupling between the $2N+2N$ and $3N+N$ channels can be neglected or is very small. Furthermore, the tensor interaction makes the energy splitting of the 0^- , 2^- and 1^- negative parity states of ^4He consistent with experiment. No such splitting is however reproduced with the effective interaction.

We believe that the physical picture obtained in the large model space with the realistic interaction should be close to the real physical situation. It is needless to say that *ab-initio* reaction calculations are very important to understand the underlying reaction dynamics involving continuum states. Simpler calculations using effective interactions in the same framework, as carried out in the present paper, are also meaningful because we can understand more clearly the effect of the tensor force by comparing both calculations. The reaction calculations with the microscopic cluster model, whose model space and interactions are restricted, have been successfully applied to many heavier nuclei. Therefore, it is instructive to see the difference from the realistic interaction by employing a simple conventional effective interaction as MN in the few-nucleon systems.

It will be quite interesting to see the importance of the tensor force in reaction observables of four nucleons. As a direct application of the present study the radiative capture reaction $d(d, \gamma)^4\text{He}$ at energies of astrophysical interest is of prime importance. It is expected to take place predominantly via $E2$ transitions [42, 27, 43, 20, 9]. As is seen from Table 1, the two deuterons can approach each other in the S -wave only when J^π is either 0^+ (1S_0) or 2^+ (5S_2). The former case is excluded because a radiative capture reaction of $0^+ \rightarrow 0^+$ is forbidden in the lowest-order electromagnetic interaction, and hence the $E2$ transition should be predominant. If there were no tensor force present, the radiative capture would be suppressed near $E = 0$ because neither d nor ^4He would have a D -wave component in contradiction with the flat behavior of the astrophysical S -factor [44]. The tensor force strongly changes this story because it can couple S - and D -waves, bringing a significant amount of D -state probability in both ^4He and d . Details of this analysis will be reported elsewhere.

Acknowledgment

We thank Dr. R. Kamouni for helpful discussions based on his PhD thesis

(in French). This work presents research results of Bilateral Joint Research Projects of the JSPS (Japan) and the FNRS (Belgium). Y. S. is supported by a Grant-in-Aid for Scientific Research (No. 21540261). This text presents research results of the Belgian program P6/23 on interuniversity attraction poles initiated by the Belgian-state Federal Services for Scientific, Technical and Cultural Affairs (FSTC). D. B. and P. D. also acknowledge travel support of the Fonds de la Recherche Scientifique Collective (FRSC). The part of computational calculations were carried out in T2K-Tsukuba.

Appendix A: Definitions of recoupling coefficients

We define an auxiliary coefficient Z that appears in the coupling

$$[[Y_a(\mathbf{e}_1)Y_b(\mathbf{e}_1)Y_b(\mathbf{e}_2)]_0]_a \rightarrow Z(ab)[Y_{a+b}(\mathbf{e}_1)Y_b(\mathbf{e}_2)]_a. \quad (\text{A.1})$$

By introducing a coefficient

$$C(ab, c) = \sqrt{\frac{(2a+1)(2b+1)}{4\pi(2c+1)}} \langle a \ 0 \ b \ 0 | c \ 0 \rangle \quad (\text{A.2})$$

for the coupling $[Y_a(\mathbf{e}_1)Y_b(\mathbf{e}_1)]_c = C(ab, c)Y_c(\mathbf{e}_1)$, we can express Z as

$$Z(ab) = \sqrt{\frac{2(a+b)+1}{(2a+1)(2b+1)}} C(ab, a+b) = \frac{1}{\sqrt{4\pi}} \langle a \ 0 \ b \ 0 | a+b \ 0 \rangle. \quad (\text{A.3})$$

Note that $C(ab, c)$ vanishes unless $a+b+c$ is even.

The coefficients that appear in Sect. 4 are given as follows:

$$X(a \ b \ c) = Z(ab)Z(ac)C(bc, b+c)U(a+c \ c \ a+b \ b; \ a \ b+c), \quad (\text{A.4})$$

$$R_3(a \ b \ c) = Z(ab)Z(a+b \ c), \quad (\text{A.5})$$

$$W(a \ b \ c \ q \ Q, \ a' \ b' \ c' \ q' \ Q', \ \ell \ \ell')$$

$$= \begin{bmatrix} q & c & Q \\ q' & c' & Q' \\ \ell' & c+c' & \ell \end{bmatrix} \begin{bmatrix} a & b & q \\ a' & b' & q' \\ a+a' & b+b' & \ell' \end{bmatrix} C(aa', a+a')C(bb', b+b')C(cc', c+c'). \quad (\text{A.6})$$

Appendix B: Matrix elements for various operators

The purpose of this appendix is to collect formulas for various matrix elements. The main procedure to derive the formulas is sketched in Sect. 4. More details for the case of two global vectors are given in Ref. [7].

B.1 Kinetic energy

Let $\boldsymbol{\pi}_j$ denote the momentum operator conjugate to \mathbf{x}_j , $\boldsymbol{\pi}_j = -i\hbar\frac{\partial}{\partial\mathbf{x}_j}$. The total kinetic energy operator for the N -nucleon system with its center of mass kinetic energy being subtracted takes the form

$$\sum_{i=1}^N \frac{\mathbf{p}_i^2}{2m} - \frac{\boldsymbol{\pi}_N^2}{2Nm} = \frac{1}{2} \tilde{\boldsymbol{\pi}} \Lambda \boldsymbol{\pi}, \quad (\text{B.1})$$

where $\boldsymbol{\pi}_N = \sum_{i=1}^N \mathbf{p}_i$ is the total momentum, $\tilde{\boldsymbol{\pi}} = (\boldsymbol{\pi}_1, \boldsymbol{\pi}_2, \dots, \boldsymbol{\pi}_{N-1})$, and Λ is an $(N-1) \times (N-1)$ symmetric mass matrix. Defining $N-1$ -dimensional column vectors Γ_i as

$$\begin{aligned} \Gamma_i &= A'B^{-1}u_i & (i=1, 2, 3), \\ \Gamma_i &= -AB^{-1}u_i & (i=4, 5, 6) \end{aligned} \quad (\text{B.2})$$

and an $(N-1) \times (N-1)$ matrix Q

$$Q_{ij} = 2\tilde{\Gamma}_i \Lambda \Gamma_j, \quad (\text{B.3})$$

we can calculate the matrix element for the kinetic energy through the overlap matrix element

$$\langle F' | \frac{1}{2} \tilde{\pi} \Lambda \pi | F \rangle = \frac{\hbar^2}{2} \left(R - \sum_{i < j} Q_{ij} \frac{\partial}{\partial \rho_{ij}} \right) \langle F' | F \rangle, \quad (\text{B.4})$$

where

$$R = 3\text{Tr}(B^{-1} A' \Lambda A). \quad (\text{B.5})$$

The ρ_{ij} values are defined in Eq. (4.11).

B.2 δ -function

A two-body interaction $V(\mathbf{r}_i - \mathbf{r}_j)$ can be expressed as

$$V(\mathbf{r}_i - \mathbf{r}_j) = \int d\mathbf{r} V(\mathbf{r}) \delta(\mathbf{r}_i - \mathbf{r}_j - \mathbf{r}). \quad (\text{B.6})$$

Once the matrix element of $\delta(\mathbf{r}_i - \mathbf{r}_j - \mathbf{r})$ is obtained, the matrix element of the interaction is calculated by integrating over \mathbf{r} the δ -function matrix element weighted with the form factor $V(\mathbf{r})$. Similarly, for a one-body operator

$$D(\mathbf{r}_i - \mathbf{x}_N) = \int d\mathbf{r} D(\mathbf{r}) \delta(\mathbf{r}_i - \mathbf{x}_N - \mathbf{r}), \quad (\text{B.7})$$

its matrix element can be obtained from that of the δ -function. Because both $\mathbf{r}_i - \mathbf{r}_j$ and $\mathbf{r}_i - \mathbf{x}_N$ can be expressed in terms of a linear combination of the relative coordinate \mathbf{x}_i , it is enough to calculate the matrix element of $\delta(\tilde{w}\mathbf{x} - \mathbf{r})$, where $\tilde{w} = (w_1, w_2, \dots, w_{N-1})$ is a combination constant to express $\mathbf{r}_i - \mathbf{r}_j$ or $\mathbf{r}_i - \mathbf{x}_N$.

The matrix element of the δ -function is given by

$$\begin{aligned} & \langle F' | \delta(\tilde{w}\mathbf{x} - \mathbf{r}) | F \rangle \\ &= \left(\frac{(2\pi)^{N-1}}{\det B} \right)^{3/2} \left(\prod_{i=1}^6 B_{L_i} \right) \frac{(-1)^{L_1+L_2+L_3} \sqrt{2L+1}}{\sqrt{2L'+1}} \left(\frac{c}{2\pi} \right)^{3/2} e^{-\frac{1}{2}c\mathbf{r}^2} \\ & \times \sum_{\kappa\mu} \langle LM\kappa\mu | L' M' \rangle Y_{\kappa\mu}^*(\hat{\mathbf{r}}) \sum_{p_i} \left(\prod_{i=1}^6 (-c\gamma_i r)^{p_i} \frac{\sqrt{2p_i+1}}{B_{p_i}} \right) \\ & \times \sum_{\ell_{12}\ell_{45}\ell'\bar{\ell}'\bar{L}_{12}\bar{L}_{45}\bar{L}} \frac{(-1)^{\ell+\ell'}}{\sqrt{(2\ell+1)(2\bar{L}+1)}} U(L\bar{L}\kappa\ell'; \ell L') \bar{O}(p_i; \ell_{12}\ell_{45}\ell'\kappa) \\ & \times W(p_1 p_2 p_3 \ell_{12} \ell, L_1 - p_1 \ L_2 - p_2 \ L_3 - p_3 \ \bar{L}_{12} \bar{L}, LL_{12}) \\ & \times W(p_4 p_5 p_6 \ell_{45} \ell', L_4 - p_4 \ L_5 - p_5 \ L_6 - p_6 \ \bar{L}_{45} \bar{L}, L' L_{45}) \\ & \times \sum_{n_{ij}} \left(\prod_{i < j} (-\bar{\rho}_{ij})^{n_{ij}} \frac{\sqrt{2n_{ij}+1}}{B_{n_{ij}}} \right) \\ & \times O(n_{ij}; L_1 - p_1 \ L_2 - p_2 \ L_3 - p_3 \ L_4 - p_4, L_5 - p_5 \ L_6 - p_6, \bar{L}_{12} \bar{L}_{45} \bar{L}), \end{aligned} \quad (\text{B.8})$$

with

$$c = (\tilde{w} B^{-1} w)^{-1}, \quad \gamma_i = \tilde{w} B^{-1} u_i, \quad \bar{\rho}_{ij} = \rho_{ij} - c\gamma_i \gamma_j. \quad (\text{B.9})$$

The summation over non-negative integers n_{ij} and p_i is restricted by the following equations

$$\begin{aligned} n_{12} + n_{13} + n_{14} + n_{15} + n_{16} + p_1 &= L_1, \\ n_{12} + n_{23} + n_{24} + n_{25} + n_{26} + p_2 &= L_2, \\ n_{13} + n_{23} + n_{34} + n_{35} + n_{36} + p_3 &= L_3, \\ n_{14} + n_{24} + n_{34} + n_{45} + n_{46} + p_4 &= L_4, \\ n_{15} + n_{25} + n_{35} + n_{45} + n_{56} + p_5 &= L_5, \\ n_{16} + n_{26} + n_{36} + n_{46} + n_{56} + p_6 &= L_6. \end{aligned} \quad (\text{B.10})$$

Here $\overline{O}(p_i; \ell_{12}\ell_{45}\ell'\kappa)$ is defined as a coefficient that appears in the coupling of a product of six terms

$$\begin{aligned} \prod_{i=1}^6 [Y_{p_i}(\mathbf{e}_i) Y_{p_i}(\widehat{\mathbf{r}})]_{00} &= \sum_{\ell_{12}\ell_{45}\ell'\kappa} \overline{O}(p_i; \ell_{12}\ell_{45}\ell'\kappa) \\ &\times \left[[Y_{p_1}(\mathbf{e}_1) Y_{p_2}(\mathbf{e}_2)]_{\ell_{12}} Y_{p_3}(\mathbf{e}_3) \right]_{\ell} \left[[Y_{p_4}(\mathbf{e}_4) Y_{p_5}(\mathbf{e}_5)]_{\ell_{45}} Y_{p_6}(\mathbf{e}_6) \right]_{\ell'} Y_{\kappa}(\widehat{\mathbf{r}})_{00}, \end{aligned} \quad (\text{B.11})$$

and it is given by

$$\begin{aligned} &\overline{O}(p_i; \ell_{12}\ell_{45}\ell'\kappa) \\ &= \sqrt{\frac{2\kappa+1}{\prod_{i=1}^6 (2p_i+1)}} C(p_1 p_2, \ell_{12}) C(\ell_{12} p_3, \ell) C(p_4 p_5, \ell_{45}) C(\ell_{45} p_6, \ell') C(\ell \ell', \kappa). \end{aligned} \quad (\text{B.12})$$

The \mathbf{r} -dependence of the matrix element (B.8) is

$$e^{-\frac{1}{2}cr^2} r^{p_1+p_2+p_3+p_4+p_5+p_6} Y_{\kappa\mu}^*(\widehat{\mathbf{r}}). \quad (\text{B.13})$$

For a central interaction, $V(\mathbf{r})$ is a scalar function, and the sum over κ in Eq. (B.8) is limited to 0. For a tensor interaction, the angular dependence of $V(\mathbf{r})$ is proportional to $Y_2(\widehat{\mathbf{r}})$, and κ is limited to 2. The electric multipole operator is a special case of one-body operator, so that one can make use of the formula (B.8) to calculate its matrix element. More explicitly, we give the matrix element of $V(|\widetilde{w}\mathbf{x}|) Y_{\kappa\mu}(\widehat{w\mathbf{x}})$ that includes all the cases mentioned above:

$$\begin{aligned} &\langle F' | V(|\widetilde{w}\mathbf{x}|) Y_{\kappa\mu}(\widehat{w\mathbf{x}}) | F \rangle \\ &= \left(\frac{(2\pi)^{N-1}}{\det B} \right)^{3/2} \left(\prod_{i=1}^6 B_{L_i} \right) \frac{(-1)^{L_1+L_2+L_3} \sqrt{2L+1}}{\sqrt{2L'+1}} \\ &\times \langle LM\kappa\mu | L'M' \rangle \sum_{p_i} \left(\prod_{i=1}^6 (-\gamma_i)^{p_i} \frac{\sqrt{2p_i+1}}{B_{p_i}} \right) \mathcal{I}_{p_1+p_2+p_3+p_4+p_5+p_6}^{(2)}(c) \\ &\times \sum_{\ell_{12}\ell_{45}\ell'\bar{L}_{12}\bar{L}_{45}\bar{L}} \frac{(-1)^{\ell+\ell'}}{\sqrt{(2\ell+1)(2\bar{L}+1)}} U(L\bar{L}\kappa\ell'; \ell L') \overline{O}(p_i; \ell_{12}\ell_{45}\ell'\kappa) \\ &\times W(p_1 p_2 p_3 \ell_{12} \ell, L_1 - p_1 \ L_2 - p_2 \ L_3 - p_3 \ \bar{L}_{12} \bar{L}, LL_{12}) \\ &\times W(p_4 p_5 p_6 \ell_{45} \ell', L_4 - p_4 \ L_5 - p_5 \ L_6 - p_6 \ \bar{L}_{45} \bar{L}, L' L_{45}) \\ &\times \sum_{n_{ij}} \left(\prod_{i<j}^6 (-\bar{\rho}_{ij})^{n_{ij}} \frac{\sqrt{2n_{ij}+1}}{B_{n_{ij}}} \right) \\ &\times O(n_{ij}; L_1 - p_1 \ L_2 - p_2 \ L_3 - p_3 \ L_4 - p_4, L_5 - p_5 \ L_6 - p_6, \bar{L}_{12} \bar{L}_{45} \bar{L}), \end{aligned} \quad (\text{B.14})$$

with the integral of the potential form factor

$$\mathcal{I}_n^{(m)}(c) = \left(\frac{c}{2\pi} \right)^{3/2} c^n \int_0^\infty dr r^{n+m} V(r) e^{-\frac{1}{2}cr^2}. \quad (\text{B.15})$$

In case $V(r)$ takes the form of $r^q e^{-\rho r^2 - \rho' r}$ ($q \geq -m$), the integral $\mathcal{I}_n^{(m)}(c)$ can be obtained analytically, giving a closed form for the matrix element.

It should be noted that the matrix element for a special class of a three-body force can be evaluated with ease. For example, if the radial part of the three-body force has a form

$$V_{TNF} = \exp(-\rho_1(\mathbf{r}_i - \mathbf{r}_j)^2 - \rho_2(\mathbf{r}_j - \mathbf{r}_k)^2 - \rho_3(\mathbf{r}_k - \mathbf{r}_i)^2), \quad (\text{B.16})$$

the exponent can be rewritten as $-\widetilde{\mathbf{x}}\Omega\mathbf{x}$ with an $(N-1) \times (N-1)$ symmetric matrix $\Omega = \rho_1 w_{ij} \widetilde{w}_{ij} + \rho_2 w_{jk} \widetilde{w}_{jk} + \rho_3 w_{ki} \widetilde{w}_{ki}$, where w_{ij} , w_{jk} and w_{ki} are defined by $\mathbf{r}_i - \mathbf{r}_j = \widetilde{w}_{ij}\mathbf{x}$, $\mathbf{r}_j - \mathbf{r}_k = \widetilde{w}_{jk}\mathbf{x}$ and $\mathbf{r}_k - \mathbf{r}_i = \widetilde{w}_{ki}\mathbf{x}$. Thus the matrix element reduces to that of the overlap with A being replaced with $A + 2\Omega$

$$\langle F' | V_{TNF} | F \rangle = \langle F' | F_{L_1 L_2 (L_{12}) L_3 L M}(u_1, u_2, u_3, A + 2\Omega, \mathbf{x}) \rangle. \quad (\text{B.17})$$

B.3 Spin-orbit potential

The spatial form of a spin-orbit interaction reads

$$V(|\mathbf{r}_i - \mathbf{r}_j|)(\mathbf{r}_i - \mathbf{r}_j) \times \frac{1}{2}(\mathbf{p}_i - \mathbf{p}_j)_\mu, \quad (\text{B.18})$$

where $(\mathbf{a} \times \mathbf{b})_\mu$ ($\mu = 0, \pm 1$) stands for the μ th component of a vector product of \mathbf{a} and \mathbf{b} . As in the δ -function matrix element, the spin-orbit potential is written as

$$V(|\tilde{w}\mathbf{x}|)(\tilde{w}\mathbf{x} \times \tilde{\zeta}\boldsymbol{\pi})_\mu, \quad (\text{B.19})$$

where $\frac{1}{2}(\mathbf{p}_i - \mathbf{p}_j)$ is expressed in terms of the momentum operators $\boldsymbol{\pi}$, $\tilde{\zeta}\boldsymbol{\pi} = \sum_{i=1}^{N-1} \zeta_i \boldsymbol{\pi}_i$.

The matrix element of the spin-orbit potential is given by

$$\begin{aligned} & \langle F' | V(|\tilde{w}\mathbf{x}|)(\tilde{w}\mathbf{x} \times \tilde{\zeta}\boldsymbol{\pi})_\mu | F \rangle \\ &= \frac{4\pi\sqrt{2}\hbar}{3} \left(\frac{(2\pi)^{N-1}}{\det B} \right)^{3/2} \left(\prod_{i=1}^6 B_{L_i} \right) \frac{(-1)^{L_1+L_2+L_3}\sqrt{2L+1}}{\sqrt{2L'+1}} \\ & \times \langle LM1\mu | L'M' \rangle \sum_{p_i} \left(\prod_{i=1}^6 (-\gamma_i)^{p_i} \frac{\sqrt{2p_i+1}}{B_{p_i}} \right) \mathcal{I}_{p_1+p_2+p_3+p_4+p_5+p_6}^{(3)}(c) \\ & \times \sum_{\ell_{12}\ell_{45}\ell\ell'\bar{\ell}_{12}\bar{\ell}_{45}\bar{\ell}'\bar{\ell}'\bar{L}_{12}\bar{L}_{45}\bar{L}} \frac{(-1)^{\bar{\ell}+\bar{\ell}'}}{\sqrt{(2\bar{\ell}+1)(2\bar{L}+1)}} U(L\bar{L}1\bar{\ell}'; \bar{\ell}L') \bar{O}(p_i; \ell_{12}\ell_{45}\ell\ell'1) \\ & \times \sum_{k=1}^6 (\tilde{\zeta}\Gamma)_k T_k(p_i, \ell_{12}\ell_{45}\ell\ell', \bar{\ell}_{12}\bar{\ell}_{45}\bar{\ell}\bar{\ell}') \sum_{n_{ij}} \left(\prod_{i<j}^6 (-\bar{\rho}_{ij})^{n_{ij}} \frac{\sqrt{2n_{ij}+1}}{B_{n_{ij}}} \right) \\ & \times O(n_{ij}; L_1-p_1^k L_2-p_2^k L_3-p_3^k L_4-p_4^k L_5-p_5^k L_6-p_6^k, \bar{L}_{12}\bar{L}_{45}\bar{L}), \end{aligned} \quad (\text{B.20})$$

where p_i^k ($k = 1, 2, \dots, 6$) is

$$p_i^k = p_i + \delta_{ik}, \quad (\text{B.21})$$

and where the non-negative integers n_{ij} and p_i are constrained to satisfy the equations

$$\begin{aligned} n_{12} + n_{13} + n_{14} + n_{15} + n_{16} + p_1^k &= L_1, \\ n_{12} + n_{23} + n_{24} + n_{25} + n_{26} + p_2^k &= L_2, \\ n_{13} + n_{23} + n_{34} + n_{35} + n_{36} + p_3^k &= L_3, \\ n_{14} + n_{24} + n_{34} + n_{45} + n_{46} + p_4^k &= L_4, \\ n_{15} + n_{25} + n_{35} + n_{45} + n_{56} + p_5^k &= L_5, \\ n_{16} + n_{26} + n_{36} + n_{46} + n_{56} + p_6^k &= L_6. \end{aligned} \quad (\text{B.22})$$

The symbol $(\tilde{\zeta}\Gamma)_k$ stands for the factor

$$(\tilde{\zeta}\Gamma)_k = \sum_{i=1}^6 \zeta_i (\Gamma_k)_i, \quad (\text{B.23})$$

where $(\Gamma_k)_i$ is the i th element of the column vector Γ_k defined in Eq. (B.2). The coefficient T_k appears in the coupling

$$\begin{aligned} & [Y_1(\mathbf{e}_k) [[[Y_{p_1}(\mathbf{e}_1)Y_{p_2}(\mathbf{e}_2)]_{\ell_{12}} Y_{p_3}(\mathbf{e}_3)]_{\ell} [[Y_{p_4}(\mathbf{e}_4)Y_{p_5}(\mathbf{e}_5)]_{\ell_{45}} Y_{p_6}(\mathbf{e}_6)]_{\ell'}]]_{1\mu} \\ & \rightarrow \sum_{\bar{\ell}_{12}\bar{\ell}_{45}\bar{\ell}\bar{\ell}'} T_k(p_i, \ell_{12}\ell_{45}\ell\ell', \bar{\ell}_{12}\bar{\ell}_{45}\bar{\ell}\bar{\ell}') \\ & \quad \times [[[Y_{p_1}^k(\mathbf{e}_1)Y_{p_2}^k(\mathbf{e}_2)]_{\bar{\ell}_{12}} Y_{p_3}^k(\mathbf{e}_3)]_{\bar{\ell}} [[Y_{p_4}^k(\mathbf{e}_4)Y_{p_5}^k(\mathbf{e}_5)]_{\bar{\ell}_{45}} Y_{p_6}^k(\mathbf{e}_6)]_{\bar{\ell}'}]]_{1\mu}. \end{aligned} \quad (\text{B.24})$$

The coefficients $T_k(p_i, \ell_{12}\ell_{45}\ell\ell', \bar{\ell}_{12}\bar{\ell}_{45}\bar{\ell}\bar{\ell}')$ are given below:

$$\begin{aligned}
T_1 &= U(1\ell 1\ell'; \bar{\ell} 1)U(1\ell_{12}\bar{\ell}p_3; \bar{\ell}_{12}\ell)U(1p_1\bar{\ell}_{12}p_2; p_1+1 \ell_{12})C(1p_1; p_1+1) \\
T_2 &= -(-1)^{\ell_{12}+\bar{\ell}_{12}}U(1\ell 1\ell'; \bar{\ell} 1)U(1\ell_{12}\bar{\ell}p_3; \bar{\ell}_{12}\ell)U(1p_2\bar{\ell}_{12}p_1; p_2+1 \ell_{12})C(1p_2; p_2+1) \\
T_3 &= -(-1)^{\ell+\bar{\ell}}U(1\ell 1\ell'; \bar{\ell} 1)U(1p_3\bar{\ell}\ell_{12}; p_3+1\ell)C(1p_3; p_3+1) \\
T_4 &= (-1)^{\ell'+\bar{\ell}'}U(1\ell' 1\ell; \bar{\ell}' 1)U(1\ell_{45}\bar{\ell}' p_4; \bar{\ell}_{45}\ell')U(1p_4\bar{\ell}_{45}p_5; p_4+1 \ell_{45})C(1p_4; p_4+1) \\
T_5 &= -(-1)^{\ell'+\bar{\ell}'+\ell_{45}+\bar{\ell}_{45}}U(1\ell' 1\ell; \bar{\ell}' 1)U(1\ell_{45}\bar{\ell}' p_6; \bar{\ell}_{45}\ell')U(1p_5\bar{\ell}_{45}p_4; p_5+1 \ell_{45})C(1p_5; p_5+1) \\
T_6 &= -U(1\ell' 1\ell; \bar{\ell}' 1)U(1p_6\bar{\ell}' \ell_{45}; p_6+1 \ell')C(1p_6; p_6+1). \tag{B.25}
\end{aligned}$$

Appendix C: Momentum representation of correlated Gaussian basis

The Fourier transform of the correlated Gaussian function (3.9) defines the corresponding basis function in momentum space. The momentum space function is useful to evaluate those matrix elements which depend on the momentum operator [7]. Suppose that we want to evaluate the matrix element of a two-body operator $V(\mathbf{p}_i - \mathbf{p}_j)$ or a one-body operator $D(\mathbf{p}_i - \frac{1}{N}\boldsymbol{\pi}_N)$. Obviously evaluating the matrix element can be done more easily in momentum space. For this purpose we need to obtain the Fourier transform of the coordinate space function. A great advantage in the correlated Gaussian function F is that its Fourier transform is a linear combination of the correlated Gaussian functions in the momentum space. Thus by expressing $\mathbf{p}_i - \mathbf{p}_j$ or $\mathbf{p}_i - \frac{1}{N}\boldsymbol{\pi}_N$ as $\tilde{\zeta}\boldsymbol{\pi}$, we can calculate the matrix element of the momentum-dependent operators in exactly the same way as in the coordinate space.

As in the case with two global vectors [7], the transformation from the coordinate to momentum space is achieved by a function

$$\Phi(\mathbf{k}, \mathbf{x}) = \frac{1}{(2\pi)^{\frac{3}{2}(N-1)}} \exp(i\tilde{\mathbf{k}}\mathbf{x}), \tag{C.1}$$

where \mathbf{k} is an $(N-1)$ -dimensional column vector whose i th element is \mathbf{k}_i . With a straightforward integration together with the recoupling of angular momenta, we can show that

$$\begin{aligned}
&\langle \Phi(\mathbf{k}, \mathbf{x}) | F_{L_1 L_2 (L_{12}) L_3 L M}(u_1, u_2, u_3, A, \mathbf{x}) \rangle \\
&= \frac{(-i)^{L_1+L_2+L_3}}{(\det A)^{3/2}} \sum_{\ell_1 \ell_2 \ell_3 \ell_{12}} \mathcal{K}(L_1 L_2 (L_{12}) L_3 L; \ell_1 \ell_2 \ell_3 \ell_{12}) \\
&\quad \times F_{L_1-\ell_1-\ell_2 \ L_2-\ell_1-\ell_3 \ (\ell_{12}) \ L_3-\ell_2-\ell_3 \ L M}(A^{-1}u_1, A^{-1}u_2, A^{-1}u_3, A^{-1}\mathbf{k}), \tag{C.2}
\end{aligned}$$

where the coefficient \mathcal{K} is given by

$$\begin{aligned}
&\mathcal{K}(L_1 L_2 (L_{12}) L_3 L; \ell_1 \ell_2 \ell_3 \ell_{12}) \\
&= \frac{(-1)^{L-L_3+\ell_2+\ell_3-\ell_{12}}}{\sqrt{2L+1}} \frac{B_{L_1} B_{L_2} B_{L_3}}{B_{\ell_1} B_{\ell_2} B_{\ell_3} B_{L_1-\ell_1-\ell_2} B_{L_2-\ell_1-\ell_3} B_{L_3-\ell_2-\ell_3}} \\
&\quad \times \sqrt{(2\ell_1+1)(2\ell_2+1)(2\ell_3+1)(2(L_1-\ell_1-\ell_2)+1)(2(L_2-\ell_1-\ell_3)+1)(2(L_3-\ell_2-\ell_3)+1)} \\
&\quad \times X(\ell_1 \ell_2 \ell_3) Z(L_1-\ell_1-\ell_2 \ \ell_1+\ell_2) Z(L_2-\ell_1-\ell_3 \ \ell_1+\ell_3) Z(L_3-\ell_2-\ell_3 \ \ell_2+\ell_3) \\
&\quad \times U(\ell_{12} \ L_3-\ell_2-\ell_3 \ L_{12} \ L_3; L \ \ell_2+\ell_3) \begin{bmatrix} L_1-\ell_1-\ell_2 & L_1 & \ell_1+\ell_2 \\ L_2-\ell_1-\ell_3 & L_2 & \ell_1+\ell_3 \\ \ell_{12} & L_{12} & \ell_2+\ell_3 \end{bmatrix} \\
&\quad \times (\tilde{u}_1 A^{-1} u_2)^{\ell_1} (\tilde{u}_1 A^{-1} u_3)^{\ell_2} (\tilde{u}_2 A^{-1} u_3)^{\ell_3}, \tag{C.3}
\end{aligned}$$

where Z and X are defined in Appendix A. Non-negative integers ℓ_i run over all possible values that satisfy $\ell_1+\ell_2 \leq L_1$, $\ell_1+\ell_3 \leq L_2$, $\ell_2+\ell_3 \leq L_3$. The value of ℓ_{12} is restricted by the triangular relations among $(\ell_{12}, L_1-\ell_1-\ell_2, L_2-\ell_1-\ell_3)$ and $(\ell_{12}, L_{12}, \ell_2+\ell_3)$.

References

1. Wildermuth K, Tang Y C (1977) A Unified Theory of the Nucleus (Vieweg, Braunschweig).

2. Kamada H, Nogga A, Glöckle W, Hiyama E, Kamimura M *et al.* (2001) Phys Rev 64:044001
3. Varga K, Suzuki Y, R. G. Lovas (1994) Nucl Phys A 571:447
4. Varga K, Ohbayasi K, Suzuki Y (1997) Phys Lett B 396:1; Varga K, Usukura J, Suzuki Y (1998) Phys Rev Lett 80:1876; Usukura J, Varga K, Suzuki Y (1998) Phys Rev A58:1918
5. Suzuki Y, Varga K (1998) Stochastic variational approach to quantum-mechanical few-body problems (Lecture notes in physics, Vol. 54). Springer, Berlin Heidelberg New York
6. Varga K, Suzuki Y (1995) Phys Rev C 52:2885
7. Suzuki Y, Horiuchi W, Orabi M, Arai K (2008) Few-Body Syst 42:33
8. Varga K, Suzuki Y, Usukura J (1998) Few-Body Syst 24:81
9. Carlson J, Schiavilla R (2008) Rev Mod Phys 70:743; Pudliner B.S, Pandharipande V.R, Carlson J, Pieper S.C, Wiringa R.B (1997) Phys Rev C 56:1720
10. Navratil P, Kamuntavicius G.P, Barrett B.R (2000) Phys Rev C 61:044001
11. Viviani M (1998) Few-Body Syst 25:197
12. Feldmeier H, Neff T, Roth R, Schnack J (1998) Nucl Phys A632:61; Neff T, Feldmeier H (2003) Nucl Phys A 713:311
13. Arai K, Aoyama S, Suzuki Y (2010) Phys Rev C 81:037301
14. Phitzinger B, Hofmann M, Hale G.M (2001) Phys Rev C 64:044003
15. Deltuva A, Fonseca A.C (2007) Phys Rev C 75:014005; Deltuva A, Fonseca A.C (2007) Phys Rev Lett 98:162502
16. Quaglioni S, Navratil P (2009) Phys Rev C 79:044606; Quaglioni S, Navratil P (2008) Phys Rev Lett 08:092501
17. Viviani M, Rosati S, Kievsky A (1998) Phys Rev Lett 81:1580; Viviani M, Kievsky A, Rosati S, George E.A, Knulson L.D (2001) Phys Rev Lett 86:3739; Viviani M, Kievsky A, Girlanda L, Marcucci L.E, Rosati S (2009) Few-Body Syst 45:119
18. Lazauskas R, Carbonell J, Fonseca A.C, Viviani M, Kievsky A, Rosati S (2005) Phys Rev C 71:034004
19. Fisher B.M *et al.* (2006) Phys Rev C 74:034001
20. Arriaga A, Pandharipande V.R, Schiavilla (1991) Phys Rev C 43:983
21. Sabourov K *et al.* (2004) Phys Rev C 70:064601
22. Hofmann H.M, Hale G.M (2008) Phys Rev C 77:044002
23. Hofmann H.M, Hale G.M (1997) Nucl Phys A 613:69; Hofmann H.M, Hale G.M (2003) Phys Rev C 68:021002
24. Deltuva A, Fonseca A.C (2007) Phys Rev C 76:021001; Deltuva A, Fonseca A.C, Sauer P.U (2008) Phys Lett B 660:471
25. Lazauskas R, Carbonell J (2004) Few-Body Syst 34:105
26. Ciesielski F, Carbonell J, Gignoux C (1999) Phys Lett B 447:199
27. Assenbaum H.J, Langanke K (1987) Phys Rev C 36:17
28. Fowler W.A, Caughlan, Zimmernman (1967) Annu Rev Astron Astrophys 5:525
29. Baye D, Heenen P H, Libert-Heinemann M (1977) Nucl Phys A 291:230
30. Kanada H, Kaneko T, Saito S, Tang Y C (1985) Nucl Phys A 444:209
31. Arai K, Descouvemont P, Baye D, (2001) Phys Rev C 63:044611
32. Descouvemont P, Baye D (2010) Rep Prog Phys 73:036301
33. Pudliner B S, Pandharipande V R, Carlson J, Pieper S C, Wiringa R B (1997): Phys Rev C 56, 1720
34. Hiyama E, Gibson B F, Kamimura M (2003) Phys Rev C 70:031001
35. Thompson D R, LeMere M, Tang Y C (1977) Nucl Phys A 286:53

36. Boys S F (1960) Proc R Soc London Ser A 258:402 ; Singer K (1960) *ibid.* 258:412
37. Suzuki Y, Usukura J (2000) Nucl Inst Method B 171:67
38. Suzuki Y, Usukura J, Varga K (1998) J Phys B 31:31
39. Horiuchi W, Suzuki Y (2008) Phys Rev C 78:034305
40. Tilley D R, Weller H R, Hale G M (1992), Nucl Phys A 541:1
41. Tamagaki R (1968) Prog Theor Phys 39:91
42. Santos F D, Arriaga A, Eiró A M, Tostevin J A (1985) Phys Rev C 31:707
43. Wachter B, Mertelmeier T, Hofmann H M (1988) Phys Lett B 200:246
44. Angulo C, Arnould M, Rayet M, Descouvemont P, Baye D *et al.* (1999) Nucl Phys A 656:3